Identification of amino acids in the human tetherin transmembrane domain responsible for HIV-1 Vpu interaction and susceptibility

Tomoko Kobayashi[1], Hirotaka Ode[2], Takeshi Yoshida[1, 3], Kei Sato[1], Peter Gee[1], Seiji P. Yamamoto[1, 4], Hirotaka Ebina[1], Klaus Strebel[3], Hironori Sato[2] and Yoshio Koyanagi [1]

[1]Laboratory of Viral Pathogenesis, Institute for Virus Research, Kyoto University, 53 Shogoin-kawara-cho, Sakyo-ku, Kyoto 606-8507, Japan
[2]Pathogen Genomics Center, National Institute of Infectious Diseases, 4-7-1 Gakuen, Musashimurayama, Tokyo 208-0011 Japan
[3]Laboratory of Molecular Microbiology, Viral Biochemistry Section, National Institute of Allergy and Infectious Diseases, NIH, Bethesda, Maryland 20892-0460, USA
[4]Department of Molecular and Cellular Biology, Graduate School of Biostudies, Kyoto University, Japan 53 Shogoin-kawara-cho, Sakyo-ku, Kyoto 606-8507, Japan

Corresponding author
Laboratory of Viral Pathogenesis, Institute for Virus Research, Kyoto University,
53 Shogoin-kawahara-cho, Sakyo-ku, Kyoto 606-8507, Japan
Phone: 81-75-751-4811
Fax: 81-75-751-4812
E-mail: ykoyanag@virus.kyoto-u.ac.jp

Running title
Structural basis for the tetherin and Vpu interaction

Key word
Tetherin, Vpu, HIV-1, helix-helix interaction, transmembrane domain

ABSTRACT

Tetherin, also known as BST-2/CD317/HM1.24, is an antiviral cellular protein that inhibits the release of HIV-1 particles from infected cells. HIV-1 viral protein U (Vpu) is a specific antagonist of human tetherin that might contribute to the high virulence of HIV-1. In this study we show that three amino acid (AA) residues (I34, L37, and L41) in the transmembrane (TM) domain of human tetherin are critical for the interaction with Vpu by using a live cell based assay. We also found that conservation of an additional AA at position 45 and two residues downstream of position 22, absent in monkey tetherins, are required for the antagonism by Vpu. Moreover, computer-assisted structural modeling and mutagenesis studies suggest that an alignment of these four AA residues (I34, L37, L41, and T45) on the same helical face in the TM domain is crucial for the Vpu-mediated antagonism of human tetherin. These results contribute to the molecular understanding of human tetherin specific antagonism by HIV-1 Vpu.

INTRODUCTION

Intrinsic immune molecules have been discovered in mammalian cells that restrict retrovirus replication (64). Tetherin, also known as BST-2/CD317/HM1.24, is a host factor which has been recently identified as a potent inhibitor against the release of HIV-1 particles (46, 67). The retained particles are then internalized into the endosomes/lysosomes and presumably degraded (4). HIV-1 is able to elude the tetherin-driven defense mechanism by expressing viral protein U (Vpu), which is expressed in a unique lineage of primate lentiviruses (64). Vpu is an 81-amino acid (AA) type 1 integral membrane protein encoded together with the *env* gene from a bicistronic mRNA and promotes the release of HIV-1 particles by specifically antagonizing tetherin (7, 63, 65). It has been shown that Vpu inhibits the cell surface expression of tetherin by its re-localization to the *trans*-Golgi network (TGN) and the recycling endosomes (12), and/or by targeting it for the proteosomal and/or lysosomal degradation in a beta trasducin repeat-containing protein (β-TrCP) dependent manner (10, 41). β-TrCP is a component of an E3 ubiquitin ligase complex that is also involved in the Vpu-induced proteasomal degradation of CD4 via the ER-associated degradation (ERAD) pathway (64, 65, 70). An AA alignment of representative primate lentiviral Vpus shows that they are highly variable and have functional differences (38, 57). Only Vpu from HIV-1 pandemic group M and non-pandemic group N strains, but not from HIV-1 group O and SIVcpz, can counteract human tetherin (hu-tetherin) activity (57). These studies suggested that the evolution of a fully functional anti-tetherin protein, such as the highly adapted Vpu of the group M strains, is an important prerequisite for the ongoing spread of HIV-1 in the human population. The anti-tetherin function of HIV-1 group M Vpu is highly specific to tetherin from human, chimpanzee, and gorilla (57). Vpu does not counteract tetherin homologues from different species such as mouse, rhesus macaques, and African green monkey (agm) (17, 43). Until now, research on the interplay between hu-tetherin and Vpu has been mainly limited to the AA residues within the TM which appear to be important for the interaction and susceptibility of tetherin to Vpu (10, 18, 43, 54). However, whether these reported AA residues also play a role in the Vpu association, and whether there are other determinants of the interaction, remains to be elucidated. Thus we set out to understand the parameters of the hu-tetherin-Vpu interaction.

Using bimolecular fluorescence complementation (BiFC) (31) and site-directed mutagenesis, we first identified three AA residues (I34, L37, and L41) within the TM

region of human tetherin (hu-tetherin) that are crucial for its interaction with Vpu in live cells. Substitution of any one of these AA residues leads to a significantly reduced interaction with Vpu, and also a loss of Vpu response in the virus release assay. Furthermore, structural and functional roles of these AA were addressed with molecular dynamic (MD) simulations of the TM domain of human and agm-tetherins in a lipid bilayer environment. To our knowledge, this is the first report showing the AA residues in hu-tetherin essential for interaction with Vpu in live cells, and we found that proper positioning of these residues is regulated by the presence of two upstream AA residues in the TM helix.

MATERIALS AND METHODS

Plasmids. The human, mouse, and agm *tetherin* cDNA was amplified by RT-PCR from human peripheral blood lymphocyte (PBL), NIH-3T3 or COS-7, respectively, and subcloned into Kusabira Green (KG) fragment-encoding plasmids, phmKGC-MC and phmKGN-MC (MBL). From pcDNA-Vphu, expressing a codon-optimized and Rev-independent HIV-1_{NL4-3} Vpu protein (47), an *orf* fragment of Vphu was also inserted into phmKGN-MN. A KGN-hu-tetherin fragment and KGN-Vphu were subcloned into CSII-CDF-GATEWAY-IRES-H2Kk (30). The mutated hu-, mo- and agm-tetherin DNA were created by overlap extension PCR. All constructs were confirmed by DNA sequencing. A list of fusion proteins of tetherin and Vpu is summarized in Fig. 1A.

Cell culture, transfection, and transduction. HEK293 cells or its derivatives were cultured in DMEM supplemented with 10% fetal bovine serum and antibiotics. Cells were transfected by calcium phosphate DNA precipitation or Lipofectamine 2000 reagent (Invitrogen) according to the manufacture's protocol. Stably KGN-Vpu or KGC-hu-tetherin-expressing HEK293 was generated by a lentiviral vector as described before (30). The amount of plasmid DNA for transfection was normalized to 1.4 μg per well by pcDNA3.1.

Confocal microscopy. HEK293 cells were transfected by an individual or a selected pairs of BiFC construct (0.5 μg of each plasmid). At 24 hr post-transfection, cells were stained with Hoechst33342 (Hoechst) (Invitrogen) and fixed with 2% paraformaldehyde, followed by treatment with 0.05% saponin. Cells were sequentially incubated with mAbs against GM130, p230, EEA1, Rab4, CD63, or LAMP1 (BD Transduction), followed by incubation with a goat anti-mouse IgG mAb (Molecular probes).

The recycling endsomes were visualized as previously reported (12). Cells were analyzed as described before (71). All the images were taken under similar experimental conditions (i.e., exposure time, magnification, and intensification), and image processing was also the same for all the images shown in the figure.

Immunoblot analysis. At 24 hr posttransfection, cells were lysed and the lysates were processed as described before (56). The membrane was incubated with anti-KGN, anti KGC mAb (MBL), anti-Flag mAb (Sigma), anti-Vpu or anti-p24 antibody (40, 56) and then horseradish peroxidase-conjugated goat anti-mouse immunoglobulin G (Santa Cruz Biotechnology). The immune complex was visualized using an enhanced chemiluminescence system (LAS 4000) according to the instructions provided by the manufacturer.

Flow cytometry. HEK293 cells were transfected either individually or in selected pairs of BiFC construct (0.5 µg of each plasmid), 24 hr posttransfection, harvested and analyzed as described (71).

Tetherin activity and Vpu sensitivity assays. HEK293 cells were transfected using Lipofectamine 2000 (Invitrogen) with 1 ug of pNL4-3 (WT), pNL4-3/Udel (Vpu deletion mutant) HIV-1 infectious plasmids (34), KGC-tagged tetherin and its derivative plasmids. Cells and supernatants were harvested 24 hr after transfection. The supernatants were filtered and infectious virion yields were measured using TZM-bl indicator cells, as described before (56), and given in relative light units (RLU).

Statistical analysis. The Mann-Whitney's U test and Student's t-test were used to determine statistical significance.

Construction of initial model for MD simulation of helix model of the tetherin TM domain in a lipid bilayer environment. To perform MD simulations (29), we first prepared seven initial models roughly mimicking helical structures of the tetherin TM domains (hu-tetherin, agm-tetherin, agm-LL, agm-LL/ I45T, hu-T45I, hu-delGI, and hu- delGI/T45I) under a lipid bilayer environment (28, 61). First, we constructed a helix peptide (D15 to C53 in hu-tetherin) in the range from the six-AA upstream of the TM domain (K21 to K47 in hu-tetherin to its six-AA downstream in each tetherin, using the LEaP module of AMBER9 (35, 51). In addition, acetyl- and N-methyl groups were connected to the N- and C-terminal ends of the peptide, respectively. We also prepared a bilayer membrane structure including about 120 palmitoyl-oleyl-*sn*-phosphatidyl-cholines (POPC), using VMD 1.8.7 (22). POPC is the largest component in cellular membrane of

mammalian cell (5, 68). Finally, the helical peptide was perpendicularly inserted into the membrane, and about 10,000 water molecules were placed on both sides of membrane surface using the LEaP module. In this study, we applied TIP3P water model (27) as water molecule. The AMBER ff99SB force field (20) was applied to energy and force calculations for peptide and water molecules, and the gaff (69) was used to those for POPC (26). The atom types and charges of each atom in POPC were automatically assigned using the Antechamber module of AMBER9 (35, 51).

MD simulations of the tetherin TM domain in a lipid bilayer environment. Prior to MD simulations of each of seven helix models, we performed energy minimization of the initial model and heated it until 36.85 ºC (310 Kelvin). The energy-minimization was achieved by 1,000 steps of the steepest descent method and by the subsequent 1,000 steps of the conjugated gradient method, to release steric clashes. The minimized model was subsequently heated using Langevin dynamics (39, 50) with the collision frequency of 5.0 pico-second^{-1} (10^{-12} sec) with NVT ensemble, during 0.1 nano-seconds (10^{-9} sec). Next, preliminary MD simulation was performed at 36.85 ºC under 1 atm pressure with NPT ensemble, during 0.5 nano-seconds. Temperature was controlled using Langevin dynamics (39, 50) with the collision frequency of 1.0 pico-second^{-1}. Until this step, to achieve equilibration for membrane prior to that for peptide, helical structure of the peptide was constrained. Distance of hydrogen bond pair between main chains of the helical peptide was force to be less than 3.0 Å with weak constraint by harmonic potential of 2.5 kcal/mol/Å^2. We further performed 4.5 nano-seconds of MD simulations without constraints of hydrogen bonds in the peptides.

Throughout the simulations, we also applied the following conditions. In the models, there are many highly charged atoms like phosphate groups in lipids. The highly charged nature of phosphate groups tends to prevent simulations from leading to stable structures having a nanosecond lifetime (16, 23, 44, 48). To avoid the unexpected effects, the additional weak forces were applied between hetero-atoms (N, O, and S atoms) in peptide side chain of ECL (D15-K21 or K47-E53 in hu-tetherin) and phosphorus atoms in lipids to weaken electrostatic interactions of highly charged phosphate atoms, using harmonic potential of 2.5 kcal/mol/Å^2 with equilibration distance at 7.0 Å when distance between them was less than 7.0 Å. In addition, periodic boundary condition was applied to avoid edge effects on boundary face. The Particle Mesh Ewald (PME) method (8, 9, 15) is used for calculating electrostatic energy of a periodic box. The cutoff distance of

non-bonded energy term was set to 12.0 Å. The movement of bonds involving hydrogen atoms was constrained by the SHAKE algorithm (55). The time step was set to 2.0 femto-second (10^{-15} sec). The simulations were achieved with the PMEMD module of AMBER9 (35, 51).

Last, we evaluated equilibration of the model. After 2.0 nanoseconds of MD simulation, each membrane thickness and root mean squared distance (RMSD) from heated structure got close to a certain value, respectively (Fig. S3). Furthermore, to validate equilibration of peptide conformation at C-terminal half of the TM domain (G27 to E51 in hu-tetherin), 3,000 snapshots were derived from 2.0 to 5.0 nano-seconds of MD simulation and were grouped into 5 clusters by the Bayesian algorithm (60) using AMBER Tool 1.2, in each model. Since the representative structure in the largest cluster is similar to the representative structures in the other four clusters (RMSD < 2.0 Å), we considered conformations of the C-terminal domain were well equilibrated (Table S2). In this study, among the 3,000 snapshots in each model, we selected a representative structure using the Bayesian clustering algorithm (60) to analyze its structural feature.

Comparison of three-dimensional models of the tetherin TM domains. We compared 3-D structures of the hu-tetherin TM models with those of other TM variants by the following procedure using PyMOL ver. 0.99 rc6 (Schrödinger LLC, http://www.pymol.org/). We first fitted models to the hu-tetherin model using the coordinates of main chain atoms (N, Cα, and C) around C-terminal TM domains (G27 to E51 in hu-tetherin), because agm-tetherin, hu-delGI, and hu-delGI/T45I have two-AA deletion in the N-terminal TM domains. Next, the root-mean-square distance (RMSD) values for individual AA residues were calculated using the coordinates of the main chain atoms in the fitted models.

RESULTS

Visualization of tetherin-Vpu heterodimer complexes in live cells

To detect tetherin-Vpu complexes in live cells, we used the BiFC technique (32) by ectopic expression of two fragmented monomeric KG fluorescent proteins. This technique is based on the formation of a fluorescent complex from N- and C-terminal non-fluorescent fragments, KGN and KGC, which are brought together by the association through interacting partner proteins fused to the fragments, thus allowing specific visualization of interactive complexes in live cells (66). Preceding reports have indicated that a peptide, -either tagged to the N-terminus of human tetherin (hu-tetherin) or C-terminus of Vpu does not interfere with their function and localization. Therefore we constructed the plasmid encoding the KGC fused to the N-terminal end of hu-tetherin (KGC-hu-tetherin), designated as pKGC-hu-tetherin. The plasmid encoding the KGN fused to the C-terminal end of codon optimized Vpu (KGN-Vpu), designated as pKGN-Vpu. The level of HIV-1 release inhibition by pKGC-hu-tetherin (data not shown) and its cell surface expression levels (Table 1) were equivalent to that of untagged hu-tetherin. In addition, pKGN-Vpu and untagged Vpu-expressing plasmid displayed similar levels of anti-tetherin activity (data not shown). We detected specific and significant fluorescence in cells co-expressing KGC-hu-tetherin and KGN-Vpu, but not in those expressing either KGC-hu-tetherin or KGN-Vpu alone, or KGN-Vpu and KGCstop (Fig. 1B). Immunoblot analysis confirmed expression and proper size of the individual proteins (KGC-hu-tetherin and KGN-Vpu) (Fig. 1A and 1B). KGCstop or KGNstop, which are mutants with a termination codon inserted at an upstream site to the tetherin ORF, were used as negative controls. In the fluorescent positive cells, little signal was seen at the plasma membrane, perhaps due to the down regulation of tetherin expression from the cell surface. By staining with antibodies or reagents specific for individual organelles within the cell, we detected BiFC signals from tetherin-Vpu complexes within organelles in which Vpu localization has previously been reported (42), however distribution frequencies were different (Fig.1C and data not shown). In fact, the previous study showed that little hu-tetherin was seen in vesicular compartments positive for the late endosome marker (LAMP-2), while in our study, the complexes appear to localize predominantly in $CD63^+$ and $LAMP\text{-}1^+$ late endosomes (Fig. 1C, right columns) (42). These results indicate that the BiFC assay is a useful and sensitive approach to determine Vpu-tetherin interactions.

Quantitative BiFC assay for tetherin and Vpu interaction

To quantitatively measure tetherin-Vpu heterodimer complexes, we generated a HEK 293 cell line stably expressing KGN-Vpu (Fig. 1D, bottom panel). Mean fluorescence intensity (MFI) of the reconstituted KG fluorophore, measured by flow cytometry, is directly proportional to the number of interactive complexes in the cells (32). To examine the sensitivity of the assay with respect to hu-tetherin and Vpu complexes, the KGN-Vpu cells were transfected with varying amounts of KGC-hu-tetherin plasmid DNA (Fig. 1D). The intensity of the KG BiFC signal corresponded well with the level of KGC-tetherin expression detected by an anti-KGC antibody 24 hr after transfection (Fig. 1D, lanes 2-4 as compared with the upper corresponding columns). These results demonstrate that our tetherin-Vpu BiFC assay provides sufficient sensitivity for measuring hu-tetherin-Vpu complexes.

Interaction of the TM region of hu-tetherin with Vpu

Tetherin has a unique topology : the amino terminal cytoplasmic tail (CT) is followed by a single TM region, an extracellular loop (ECL), coiled-coil domain (CC) and a glycosyl phosphatidylinositol membrane anchor (GPI) at the C-terminus (36). To map the domain of hu-tetherin that mediates interaction with Vpu, we first prepared KGC-tagged tetherin mutants deleted in the CT or GPI anchor (delCT and delGPI, Fig. 1A), transfected them into the KGN-Vpu-expressing cells, and examined the resulting BiFC signals. We found that delCT and delGPI mutants produced slightly enhanced BiFC signals as compared to wild type (WT) tetherin (Fig. 2A), perhaps due to an increase in the expression level in cells (Fig. 2A, bottom panels), or a change in the protein localization. These data reveal that the CT and GPI regions in tetherin are not required for Vpu interaction. To investigate specific characteristics of the hu-tetherin-Vpu complex under similar topological conditions, we next used KGC-tagged mouse tetherin (KGC-mo-tetherin) (Fig. 1A). Since mo-tetherin displays resistance to Vpu counteraction (17), less interaction between Vpu and mo-tetherin was expected. In fact, co-expression of KGN-Vpu and KGC-mo-tetherin gave no detectable fluorophore (Fig. 2B and C, lane 10), while co-expression of KGN-tagged mo-tetherin and KGC-mo-tetherin yielded a signal (data not shown), indicating mo-tetherin homodimer formation can produce a strong fluorophore. To further verify BiFC signals, we examined the subcellular localization of Vpu and tetherin together with BiFC signals. The results showed that hu-tetherin co-localized with Vpu as well as BiFC signals (Fig. 2B, lower

panels), whereas mo-tetherin co-localized with Vpu but did not produce BiFC florescence (Fig. 2B, upper panels). This indicated that BiFC signals are the results of specific interactions. These data suggest that specific region(s) of hu-tetherin participates in the interaction with Vpu. Thus, we next prepared KGC-tagged hu- or mo-tetherin-based chimera with substitutions of the TM, ECL, CC, and GPI from mo-tetherin or hu-tetherin (Fig. 1A). Subcellular localization and cell surface expression of the chimeric tetherins were detected by anti-KGC antibody or quantified using an anti-hu-tetherin antibody that reacts with the ECL domain, respectively. The anti-hu-tetherin antibody does not react with mouse ECL domain; thus, we were only able to quantify the cell surface expression of chimera carrying the human ECL domain. Cell surface expression and localization of these chimera were similar to that of WT hu-tetherin (**Table 1** and data not shown). Furthermore, we examined the total expression of the mutants by immunoblot analysis using an anti-KGC antibody. Expression of all chimeras was comparable (Fig. 2C). The mo-tetherin-based chimeric proteins migrate as multiple bands on immunoblot analysis, probably due to their differential N-glycosylation (1, 17). Hu-tetherin-based chimeras with ECL, CC, or GPI domains of mo-tetherin but carrying a TM domain of hu-tetherin, displayed BiFC signals comparable to that of WT hu-tetherin (Fig. 2C). By contrast, hu-tetherin-based chimera with the reciprocal TM of mo-tetherin, showed a significant reduction in BiFC signal (Fig. 2C). Conversely, mo-tetherin-based chimera with the reciprocal TM of hu-tetherin displayed significant BiFC signals comparable to parental hu-tetherin (Fig. 2C), indicating that the TM of hu-tetherin is necessary and sufficient for the interaction between mo-tetherin based mutants and Vpu. Mo-tetherin-based chimera mutants replaced with the ECL, CC, or GPI of hu-tetherin showed a weak signal (Fig. 2C), suggesting that the other regions are less important in the Vpu interaction.

Specific interaction of Vpu TM with hu-tetherin

HIV-1 Vpu protein consists of two major elements: an N-terminal TM domain that anchors Vpu in the cellular membranes and a CT consisting of two putative α-helices separated by a conserved phosphorylation site (21). To understand, which domain of Vpu interacts with hu-tetherin, we generated HEK 293 cells stably expressing KGC-tagged hu-tetherin (KGC-hu-tetherin) (Fig. 2D). Cells were transfected with plasmids encoding KGN-Vpu WT or mutants. We prepared KGN-tagged Vpu mutants by truncating its CT at residue 50 (Vpu1-50), replacing the TM region with a scrambled TM sequence (VpuRD), substituting

an alanine at serine residues 52 and 56 in the cytoplasmic domain (Vpu2/6), or by substituting positively charged residues within the putative overlapping tyrosine- and dileucine-based sorting motifs with alanine (VpuR30A/K31A) (Fig. 1A) (12, 46, 58, 59). The levels of KGN-Vpu expression of these mutants were nearly equivalent (Fig. 2D, upper panels) and did not significantly alter KGC-hu-tetherin expression (Fig. 2D, lower panels). Our BiFC assay revealed that VpuRD poorly interacted with hu-tetherin while Vpu1-50 displayed BiFC signals equivalent to WT Vpu (Fig. 2D, top columns), indicating that Vpu interacts with hu-tetherin through its TM domain. Moreover, VpuR30A/K31A displayed a modest decrease in BiFC signal. A previous study showed that the VpuR30A/K31A mutant displayed a partial (~40%) defects in its TGN localization and its efficient delivery to late endosomal degradation compartments (12). This indicates that the trafficking of Vpu to the TGN may be important, to some extent, for hu-tetherin interaction. Our results confirm that Vpu and hu-tetherin interact with each other via their respective TM regions.

Mapping of the Vpu interaction domain in hu-tetherin TM

To reveal the Vpu-interacting AA in the TM region of tetherin, we next prepared plasmids encoding KGC-tagged hu-tetherin mutants with triple-alanine-substitution in the TM region (Fig. 3A, top panel) and then transfected them into KGN-Vpu expressing cells. Alanine is the substitution residue of choice since it eliminates the side chain beyond the β-carbon and yet does not alter the main-chain conformation (as can glycine or proline) nor does it impose extreme electrostatic or steric effects (37). Levels of cell surface expression of these mutants were nearly equivalent to or greater than that of WT hu-tetherin (Table 1). The level of KGC expression detected by immunoblot analysis were equivalent to that of WT hu-tetherin (Fig. 3A, bottom panel), while LLL(22-24)AAA, IVI(34-36)AAA, LGV(37-39)AAA, and PLI(40-42)AAA showed clearly reduced BiFC signals when compared with WT hu-tetherin (Fig. 3A). These data suggest that the residues covering 22-24 and 34-42 of hu-tetherin play a crucial role in the Vpu interaction. The reduction of Vpu binding capacity by substitution of residues 22-24 in hu-tetherin might correspond to a previous observation that deletion of 22L and 23L from hu-tetherin disrupts the interaction with Vpu (54).

To narrow down interacting AA residues within the 34-42 region of hu-tetherin, we next prepared single alanine substituted mutants (Fig. 3B, top panel). The levels of cell surface protein expression of the mutants were equivalent to that of WT hu-tetherin (Table

1), and their electrophoretic mobilities were consistent with the expected sizes (Fig. 3B, bottom panel). Among the nine single alanine substituted mutants, I34A, L37A, and L41A mutations produced significantly reduced BiFC signals compared to hu-tetherin or its other mutants (Fig. 3B, right columns).

I34, L37 and L41 of hu-tetherin are involved in the determination of Vpu susceptibility

To examine whether the interaction between hu-tetherin and Vpu through I34, L37 and L41 residues play a functional role in determination of Vpu susceptibility, we tested these mutants for Vpu susceptibility and tetherin activity. HEK293 cells were transfected with infectious WT HIV-1 DNA (pNL4-3) or its Vpu-deleted HIV-1 DNA (pNL4-3/Udel) together with WT hu-tetherin or its mutants. The amount of HIV-1 in the culture supernatants together with HIV-1 protein in cell extract was determined. Importantly, hu-tetherin mutants with I34A, L37A, P40A and L41A mutations completely lost their Vpu susceptibility, while V35A, I36A, G38A, V39A, I42A remained Vpu sensitive (Fig. 3C). To determine whether mutants that conferred resistance to antagonism by Vpu in virion release assays also conferred resistance to the down regulation of tetherin from the cell surface, we examined cell surface expression of tetherin or its derivatives on these cells. In our results, the level of the tetherin down-regulation of I34A, L37A, and L41A mutants were similar to that of WT tetherin (Fig. 3D). On the other hand, only P40A displayed resistance to Vpu induced down regulation. These results suggest that different mechanisms account for the loss of Vpu sensitivity in P40 A and other mutants. Overall, these results provide direct evidence that I34, L37 and L41 of hu-tetherin are involved in the determination of Vpu susceptibility in addition to Vpu interaction. Interestingly, these AA residues are highly conserved among primate tetherins and are present not only in Vpu-sensitive but also in Vpu-insensitive tetherins (Fig. 3E, gray boxes 34, 37, and 41). This suggests that the presence of these residues alone is insufficient to render tetherin Vpu-sensitive. Indeed, a previous report demonstrated that agm-tetherin poorly interacted with HIV-1 Vpu (54). Thus, we hypothesize that the difference of Vpu interaction efficiency between hu- and agm-tetherin might be due to differences in secondary structure rather than the primary AA sequence of the TM domain. Furthermore, additional residues in human tetherin that are not conserved in monkey tetherins may contribute to Vpu sensitivity.

Acquisition of Vpu interacting activity in agm-tetherin by the insertion of two AA residues and acquisition of Vpu susceptibility by a single AA mutation

To determine additional critical AA residues that affect the Vpu interaction and susceptibility, we carried out both loss- and gain-of-function approaches using hu- or agm-tetherin. Human and chimpanzee tetherins contain a dileucine motif upstream of the Vpu binding domain that is absent in other primate tetherins (Fig. 3E). Deletion of this motif (L22 and L23) in hu-tetherin clearly influenced its Vpu binding capacity (54). Another report demonstrated that a two AA deletion and a single AA substitution in the hu-tetherin TM (hu-delGI/T45I) can confer complete resistance to antagonism by Vpu (43). Hence, we focused on these two regions for the subsequent experiments (Fig. 4A). To confirm no alteration of intracellular distribution of tetherin by deleting or inserting AA in its TM region, we examined the distribution of representative mutants (hu-delGI, agm-LL). The localizations of these mutants were very similar to that of hu-tetherin or agm-tetherin respectively (Fig. 4B).

For the loss-of-function approach from hu-tetherin, we prepared KGC-tagged hu-delGI, hu-T45I and hu-delGI/T45I tetherin mutants (Fig.4A). Although the levels of KGC expression of these mutants were equivalent to WT hu-tetherin (Fig. 4C, panels), hu-delGI and hu-delGI/T45I displayed significantly lower BiFC signals than WT hu-tetherin, while hu-T45I displayed a similar level of BiFC signals to WT hu-tetherin (Fig. 4C). Among these hu-tetherin mutants, hu-delGI/T45I showed the lowest interaction profile with Vpu. These data indicate that by itself T45 does not play a significant role in Vpu interaction; however, it exacerbates the effect of the GI deletion (G25 and I26). From tetherin activity and Vpu susceptibility assays, we confirmed that hu-delGI remained partially sensitive to Vpu (Fig. 4D) as previously described (43).

For the gain-of-function approach we prepared two KGC-tagged agm-tetherin mutants, by inserting two leucine residues (agm-LL), or by combining the insertion of two leucines with a mutation of I45T (corresponding to hu-tetherin residues) (Fig. 4A). As demonstrated in Fig. 4C, agm-LL displayed more than 2-fold increase of BiFC signal compared to WT agm-tetherin. We also tested these mutants for tetherin activity and Vpu sensitivity. Notably, an agm-LL mutant was insensitive to HIV-1 Vpu antagonism (Fig. 4D) even though it interacted with Vpu to a certain extent (Fig. 4C). Finally, the agm-LL/I45T mutant, containing the combined two leucine insertion and I45T in the TM of agm-tetherin, clearly displayed the Vpu sensitivity (Fig. 4D). However, its BiFC signal was not increased

by I45T substitution (Fig. 4C). These results suggest that T45 of hu-tetherin has an important role for Vpu counteraction against tetherin without affecting Vpu-tetherin association.

Structural study of the TM domain of hu- and agm- tetherins in a lipid bilayer environment

To obtain structural insights into the mechanisms by which the AA at specific positions in the tetherin TM domain control interaction and susceptibilities to neutralization by Vpu, we constructed three-dimensional (3-D) models of the TM domains of hu-tetherin, agm-tetherin, and five tetherin mutants including agm-LL, agm-LL/I45T, hu-delGI, hu-T45I and hu-delGI/T45I. We constructed these models in a lipid bilayer environment by MD simulations (28, 29, 61) of the models and compared the structures. Representative structures were obtained by cluster analysis (60) of the 3000 snapshots during 2.0-5.0 nanoseconds of each MD simulation for the structural comparisons. Details of the simulation methods and processes such as the time course of structural changes during MD simulations are described in the **SUPPLEMENTAL MATERIAL** (Table S1, Fig. S1, and S2).

The thermodynamically stable hu-tetherin TM model shows that the TM consists of helical structures in the lipid bilayer, consistent with its location in the plasma membrane. In the model, AA residues I34, L37, and L41, which we demonstrated above to be indispensable for Vpu interaction, are positioned on the same face of the helix in the lipid bilayer environment, leading to the protrusion of the hydrophobic side chains into a similar direction (Fig. 5A, AA residues with red color). V30, F44, T45, and A48 of hu-tetherin were also positioned on the same helical face with these AA residues (Fig. 5A, AA residues with orange color). This 3-D arrangement of particular AA on the helical surface was significantly disordered in the TM domains of the agm-tetherin; side chains of I34, L37, and L41, which correspond to the I34, L37, and L41 in hu-tetherin, respectively, protruded in separate directions (Fig. 5B, agm-tetherin). When the agm-tetherin TM model was superimposed with the hu-tetherin TM model using the main chain atoms (see **MATERIALS AND METHODS**), more than 2.0 Å of 3-D positional shifts were detected at the many main chains. This included I34, L37, F44, I45, and A48, which correspond to I34, L37, F44, T45, and A48, respectively, in hu-tetherin (Fig. 5B and S2). On the other hand, conformational changes from the hu-tetherin TM were detected ~~with~~ in the smaller

regions of other TM variants examined (Fig.5B, agm-LL, agm-LL/I45T, hu-delGI, hu-T45I, and hu-delGI/T45I). More than 2.0 Å of positional shifts were observed only at I45 of agm-LL, I34 of agm-LL/I45T, A48 of hu-T45I, and F44, I45 of hu-delGI/T45I (Fig. 5B and S2). The hu-delGI was more similar in structure to hu-tetherin than the others (Fig. 5B and S2).

Experimental data showed that I34, L37, and L41 in hu-tetherin are critical for Vpu interaction (Fig. 3B). Hence, we examined how the three-dimensional positions of these AA residues are maintained. The hu-T45I, hu-delGI, and agm-LL, which have relatively high competence for Vpu interaction, showed positional shifts of the three AA residues, were less than 1.3 Å (Fig. 5B and S2). In contrast, the others showed greater positional shifts of the three AA residues. Positions of I34 in agm-thetherin and agm-LL/I45T shifted 1.9 to 2.4 Å, while that of L41 in hu-delGI/T45I shifted 1.6 Å. These results are consistent with their competence for Vpu interaction.

Experimental data also pointed out the crucial importance of the AA residue at position 45 for the susceptibility of hu-tetherin to Vpu (Fig. 4D). The hu-tetherin and two mutants (agm-LL/I45T and hu-delGI) have threonine at this position and shared relatively similar conformation at the threonine and neighboring phenylalanine (F44 in hu-tetherin); less than 1.5 Å of positional shifts were detected when these mutant TMs were superimposed with the hu-tetherin TM (Fig. 5B and S2**)**. The conformational differences from the hu-tetherin TM were greater with those having substitution of threonine into isoleucine (agm-tetherin, agm-LL, hu-T45I, and hu-delGI/T45I); the differences ranged from 1.7 to 3.5 Å with these mutants (Fig. 5B and S2).

We also analyzed the snapshot models at 5.0 nanoseconds of each MD simulation. All of these structural characteristics and differences found with the representative models were reproducible with the snapshot model at 5.0 nanoseconds of each MD simulation (Fig. S3) where fluctuations of TM structures during MD simulations were relatively small (Fig. S1). Our structural models support the results that the Vpu specific interaction and susceptibility with hu-tetherin is defined by critical AA residues which lie in the TM (I34, L37, L41 and T45), and imply that the appropriate positioning of these AA residues in hu-tetherin are important for Vpu interaction and sensitivity.

Discussion

The molecular basis behind HIV-1 Vpu counteraction of hu-tetherin has not been fully elucidated. Despite the observation that specific antagonism of hu-tetherin occurs through a Vpu-mediated pathway, the specific residues of hu-tetherin which define the association with Vpu remain unknown. In this report, we utilized a BiFC approach to characterize the interaction between Vpu and tetherin (Fig. 1). We firstly validated our BiFC approach by detecting the specific hu-tetherin-Vpu heterodimer complexes (Fig.1B and D), which have been previously shown by immunoprecipitation studies (25, 54). The complementation-based method is a simple way for confirming the protein-protein interaction in live cells. As BiFC depends on the two interacting proteins to bring the complementary fluorescence protein fragments close enough to fold into stable fluorescence complex, a positive BiFC signal implies a distance of less than 15 nm between the two interacting proteins (33). Consistent with our BiFC results, hu-tetherin and Vpu interaction were recently reported using a fluorescence resonance energy transfer (FRET) assay (2) suggesting a distance of less than 6 nm between the interacting Vpu and tetherin (52). However, it should be noted that although the BiFC assay demonstrated a positive association of tetherin and Vpu, it remains unclear whether the interaction is direct or indirect. As a result, we were able to identify three AA residues (I34, L37 and L41) which were shown in our 3-D model to align on the same TM helical surface for Vpu interaction (Fig. 5). Altering any one of these AA residues lead to a disruption of the Vpu-hu-tetherin complex and also abrogated Vpu-susceptibility (Fig. 3). Furthermore, our finding that the T45 residue of hu-tetherin had no bearing on the Vpu interaction, yet significantly abated Vpu-susceptibility (Fig. 4), implies that certain residues participate exclusively in the Vpu-mediated antagonism of tetherin independently of the interaction. In addition, our 3-D models offer a glimpse into the possible dynamics of the viral and host molecules and allow us to visualize the arrangement of the AA residues in the hu-tetherin TM involved in the possible binding with Vpu.

Recently, several groups have demonstrated that the hu-tetherin TM and specific residues within it are essential for Vpu interaction and hu-tetherin counteraction (10). The studies identified hu-tetherin delGI T45I, delGI I33V I36L (43), del22/23 (54), T45I and I26V/V30G/I36L/T45I (18) as mutants that are resistant to Vpu, but mainly focused on hu-tetherin residues which differed from rhesus or agm- tetherin residues (10). In contrast, we conducted a comprehensive screening of the entire TM region and identified three

residues (I34, L37, or L41) as critical determinants for Vpu interaction and susceptibility (Fig.3B and C). Our model predicts that these three AA residues are directly involved in helix-helix interactions between the TMs of tetherin and Vpu, composing an interacting domain (Fig. 5A). This possibility is feasible considering the biochemical characteristics of hydrophobic isoleucine and leucine which are often located at the surfaces of protein-protein interaction sites in membrane proteins, as exemplified in leucine zipper and leucine/isoleucine zipper motifs. The deletion mutants, delGI and L22-23, respectively, had a significant impact on perturbing the Vpu-mediated antagonism of hu-tetherin (Fig. 4D). Our gain-of-function studies showed the insertion of two residues (LL) in the TM of agm-tetherin was enough to restore a partial level of interaction with Vpu, and in combination with the I45T mutation, led to a partial restoration of Vpu sensitivity (Fig. 4D). We speculate that missing residues in the helix, such as the delGI mutant and agm-tetherin, may have an overall impact on the TM AA residue positioning, thereby affecting both interaction and sensitivity. Interestingly, mutations of L22 and L23 to alanine in our triple alanine scan mutants disrupted Vpu interaction, whereas mutations of G25 and I26 to alanine did not have any effect (Fig. 3A). This finding leads us to believe that the deletion of LL may have a more specific effect on the Vpu interaction in conjunction with orienting the tetherin helix TM residues.

In an evolutionary aspect, two AA in the hu-tetherin TM might have been inserted when advanced primates evolved from primitive primates, resulting in an adaption by HIV-1 Vpu to recognize hu-tetherin. It is unclear why these insertions at position 22-23 occur in hu-tetherin, but the fact that these regions also evolved under selective pressure show that these events might have occurred as a consequence of their role in other functional activities of tetherin, such as B cell differentiation, the inhibition of virus production, or the regulation of interferon release (6, 18, 24, 43).

In contrast to other reports we could not definitively verify the importance of the mutant I36A. Mutation of I36 did not have an impact on the Vpu and hu-tetherin interaction in our BiFC assay; even though it attenuated Vpu susceptibility during virus release, the effect was not as dramatic as mutating L34, L37, L41, or T45 (Fig. 3B, 3C, 4C, and 4D). Mutants I26A and V30A were not investigated further because they did not disrupt the Vpu and tetherin BiFC fluorphore in our preliminary interaction screen (Fig. 3A).

Interestingly, a P40A mutation also abolished susceptibility to Vpu (Fig. 3C), although McNatt *et al*. reported that a P40I mutation does not affect the Vpu susceptibility

(43). However, this discrepancy is more likely due to an overall conformational rearrangement of the hu-tetherin TM from replacement of proline with hydrophobic AA of different sizes. Proline residues generally play significant roles in maintaining the conformational structure, and exchanging proline to alanine can affect the overall conformation more dramatically than exchanging proline to isoleucine (53). In addition to P40A, I36A also displayed, to a lesser extent, Vpu counteraction (Fig. 3C). In a previous study, I36 has been shown to be one of the positively selected residues in the hu-tetherin TM sequence. When this residue was exchanged for the corresponding residue found in the resusus tetherin TM, a loss of susceptibility to Vpu was observed. From our structural analysis of human tetherin, I36 is not likely to be involved in interaction, however, exchanging I36 to other residues can affect the Vpu susceptibility.

One of the more important observations of our study was the function of T45, which has repeatedly been reported to be essential for Vpu susceptibility by others. In our hands, a mutation of this residue did not significantly affect Vpu and hu-tetherin complex formation when measuring the interaction by BiFC; yet, mutation of T45 still affected Vpu sensitivity (Fig. 4D). Our gain-of-function studies further illustrated the importance of T45 by rendering agm-tetherin susceptible to Vpu in the agm-LL/I45T mutant, an effect which was not observed when examining the agm-LL mutant without the I45T substitution. This suggests that Vpu-tetherin association alone is not sufficient for acquiring antagonistic activity.

Changes in AA at position 45 in hu-tetherin TM are predicted to influence the conformation of not only itself but also its immediate downstream AA at position 44 (Fig. 5B and S2). When hu-tetherin has a threonine at position 45, AA at position 44 and 45 tended to be positioned on the same surface with the functionally important AA, such as I34, L37, and L41 (Fig. 4B and S4). Concurrent with this folding property, tetherins tended to preserve the Vpu-susceptibility (Fig. 4D: hu-delGI). In contrast, when agm-tetherin has an isoleucine at position 45, the ordered 3-D arrangement fluctuated particularly at positions 44 and 45, and the tetherins tended to have severely reduced susceptibilities to Vpu activity (Fig. 4D, 5B, Table S1, and Fig. S2). These results indicate that the AA at position 45 plays crucial roles in both folding and Vpu-susceptibility of the hu-tetherin TM domain. This is consistent with biochemical characteristics of threonine; in general, threonine is rare in TMs of proteins, however, if it exists, the threonine can play very important roles in folding and protein-protein interaction of TMs (49), such as tight packing of helices (14), formation

of inter-molecular hydrogen bonds (13, 62), and formation of biologically functional protein complexes (3). Therefore, it is conceivable that T45 in hu-tetherin plays key roles in forming a biologically functional complex of hu-tetherin, Vpu, and undefined proteins for the Vpu-mediated degradation of tetherin. T45 may play an important role in one or more of the reported mechanisms by which Vpu antagonizes hu-tetherin: (1) by targeting hu-tetherin for the proteasomal and/or lysosomal degradation via the β-TrCP dependent ubiquitin/proteasome pathway (10); (2) by trafficking hu-tetherin to intracellular organelles such as the TGN, Golgi, or ER (12); (3) by sequestering hu-tetherin within intracellular compartments and preventing its distribution to the plasma membrane (11, 19). Although our results indicate T45 to behave in this manner, residues identified by Gupta *et al*, such as I26, V30 and I36, may also, similarly, contribute. Further structural and biochemical studies are necessary to address this issue.

In conclusion, the main advantage our modeling results provide is the visualization and positioning of the TM AA residues in a manner which allows for Vpu binding. To our knowledge, this is the first 3-D model for the TM domain of tetherin that offers a plausible explanation for the residues involved in the Vpu-hu-tetherin interaction. Having this insight will aid in identifying the complementary motifs in Vpu that interact with the three AA residues found in this study. Our BiFC system will also be a useful tool for building a structure activity relationship and elucidating the Vpu TM residues contributing to tetherin binding. Moreover, it is also conceivable to design a type of peptide decoy molecule (45), consisting of only a TM domain homologous to human tetherin, able to sequester Vpu while permitting the retainment of HIV-1 virions by tetherin. With this in mind, and guided by structure based predictions, the Vpu-tetherin complex could become a novel target for future pharmacological intervention of HIV-1 dissemination.

ACKNOWLEDGEMENTS

We would like to thank Jun Komano and Chuanyi Nie for helpful discussions of the manuscript. This work was supported by Grant-in-Aid for Science Research of Priority Areas from the Ministry of Education, Culture, Sports, and Technology of Japan, and Health and Labor Science Research Grant (Research on Publicly Essential Drugs and Medical Devices) and a Grant for HIV/AIDS Research from the Ministry of Health, Labor and Welfare of Japan. K.S., T.Y., and S.P.Y. were supported by Research Fellowships from the Japan Society for the promotion of Science for Young Scientists.

REFERENCES

1. **Andrew, A. J., E. Miyagi, S. Kao, and K. Strebel.** 2009. The formation of cysteine-linked dimers of BST-2/tetherin is important for inhibition of HIV-1 virus release but not for sensitivity to Vpu. Retrovirology **6:**80.
2. **Banning, C., J. Votteler, D. Hoffmann, H. Koppensteiner, M. Warmer, R. Reimer, F. Kirchhoff, U. Schubert, J. Hauber, and M. Schindler.** 2010. A flow cytometry-based FRET assay to identify and analyse protein-protein interactions in living cells. PLoS One **5:**e9344.
3. **Beahm, D. L., A. Oshima, G. M. Gaietta, G. M. Hand, A. E. Smock, S. N. Zucker, M. M. Toloue, A. Chandrasekhar, B. J. Nicholson, and G. E. Sosinsky.** 2006. Mutation of a conserved threonine in the third transmembrane helix of alpha- and beta-connexins creates a dominant-negative closed gap junction channel. J. Biol. Chem. **281:**7994-8009.
4. **Bieniasz, P. D.** 2009. The cell biology of HIV-1 virion genesis. Cell Host Microbe **5:**550-558.
5. **Brugger, B., B. Glass, P. Haberkant, I. Leibrecht, F. T. Wieland, and H. G. Krausslich.** 2006. The HIV lipidome: a raft with an unusual composition. Proc. Natl. Acad. Sci. USA **103:**2641-2646.
6. **Cao, W., L. Bover, M. Cho, X. Wen, S. Hanabuchi, M. Bao, D. B. Rosen, Y. H. Wang, J. L. Shaw, Q. Du, C. Li, N. Arai, Z. Yao, L. L. Lanier, and Y. J. Liu.** 2009. Regulation of TLR7/9 responses in plasmacytoid dendritic cells by BST2 and ILT7 receptor interaction. J. Exp. Med. **206:**1603-1614.
7. **Cohen, E. A., E. F. Terwilliger, J. G. Sodroski, and W. A. Haseltine.** 1988. Identification of a protein encoded by the vpu gene of HIV-1. Nature **334:**532-534.
8. **Crowley, M. F., T. A. Darden, T. E. Cheatham, and D. W. Deerfield.** 1997. Adventures in improving the scaling and accuracy of a parallel molecular dynamics program. . J. Supercomput. **11:**255-278.
9. **Darden, T., D. York, and L. Pedersen.** 1993. Particle mesh Ewald--an Nlog(N) method for Ewald sums in large systems. J. Chem. Phys. **98:**10089-10092.
10. **Douglas, J. L., J. K. Gustin, K. Viswanathan, M. Mansouri, A. V. Moses, and K. Fruh.** 2010. The great escape: viral strategies to counter BST-2/tetherin. PLoS Pathog. **6:**e1000913.
11. **Dube, M., B. B. Roy, P. Guiot-Guillain, J. Binette, J. Mercier, A. Chiasson, and E. A. Cohen.** 2010. Antagonism of tetherin restriction of HIV-1 release by Vpu involves

binding and sequestration of the restriction factor in a perinuclear compartment. PLoS Pathog. **6:**e1000856.

12. **Dube, M., B. B. Roy, P. Guiot-Guillain, J. Mercier, J. Binette, G. Leung, and E. A. Cohen.** 2009. Suppression of Tetherin-restricting activity upon human immunodeficiency virus type 1 particle release correlates with localization of Vpu in the trans-Golgi network. J. Virol. **83:**4574-4590.
13. **Duong, M. T., T. M. Jaszewski, K. G. Fleming, and K. R. MacKenzie.** 2007. Changes in apparent free energy of helix-helix dimerization in a biological membrane due to point mutations. J. Mol. Biol. **371:**422-434.
14. **Eilers, M., S. C. Shekar, T. Shieh, S. O. Smith, and P. J. Fleming.** 2000. Internal packing of helical membrane proteins. Proc. Natl. Acad. Sci. USA **97:**5796-5801.
15. **Essmann, U., L. Perera, M. L. Berkowitz, T. Darden, H. Lee, and L. G. Pedersen.** 1995. A smooth particle mesh Ewald method. J. Chem. Phys. **103:**8577-8593
16. **Fritsch, V., G. Ravishanker, D. L. Beveridge, and E. Westhof.** 1993. Molecular dynamics simulations of poly(dA) · poly(dT): comparisons between implicit and explicit solvent representations. Biopolymers **33:**1537–1552.
17. **Goffinet, C., I. Allespach, S. Homann, H. M. Tervo, A. Habermann, D. Rupp, L. Oberbremer, C. Kern, N. Tibroni, S. Welsch, J. Krijnse-Locker, G. Banting, H. G. Krausslich, O. T. Fackler, and O. T. Keppler.** 2009. HIV-1 antagonism of CD317 is species specific and involves Vpu-mediated proteasomal degradation of the restriction factor. Cell Host Microbe **5:**285-297.
18. **Gupta, R. K., S. Hue, T. Schaller, E. Verschoor, D. Pillay, and G. J. Towers.** 2009. Mutation of a single residue renders human tetherin resistant to HIV-1 Vpu-mediated depletion. PLoS Pathog. **5:**e1000443.
19. **Hauser, H., L. A. Lopez, S. J. Yang, J. E. Oldenburg, C. M. Exline, J. C. Guatelli, and P. M. Cannon.** 2010. HIV-1 Vpu and HIV-2 Env counteract BST-2/tetherin by sequestration in a perinuclear compartment. Retrovirology **7:**51.
20. **Hornak, V., R. Abel, A. Okur, B. Strockbine, A. Roitberg, and C. Simmerling.** 2006. Comparison of multiple Amber force fields and development of improved protein backbone parameters. Proteins **65:**712-725.
21. **Hout, D. R., E. R. Mulcahy, E. Pacyniak, L. M. Gomez, M. L. Gomez, and E. B. Stephens.** 2004. Vpu: a multifunctional protein that enhances the pathogenesis of human immunodeficiency virus type 1. Curr. HIV Res. **2:**255-270.

22. **Humphrey, W., A. Dalke, and K. Schulten.** 1996. VMD: visual molecular dynamics. J. Mol. Graph. **14:**33-38, 27-38.

23. **Ibragimova, G. T., and R. C. Wade.** 1998. Importance of explicit salt ions for protein stability in molecular dynamics simulation. Biophys. J. **74:**2906-2911.

24. **Ishikawa, J., T. Kaisho, H. Tomizawa, B. O. Lee, Y. Kobune, J. Inazawa, K. Oritani, M. Itoh, T. Ochi, K. Ishihara, and et al.** 1995. Molecular cloning and chromosomal mapping of a bone marrow stromal cell surface gene, BST2, that may be involved in pre-B-cell growth. Genomics **26:**527-534.

25. **Iwabu, Y., H. Fujita, M. Kinomoto, K. Kaneko, Y. Ishizaka, Y. Tanaka, T. Sata, and K. Tokunaga.** 2009. HIV-1 accessory protein Vpu internalizes cell-surface BST-2/tetherin through transmembrane interactions leading to lysosomes. J. Biol. Chem. **284:**35060-35072.

26. **Jojart, B., and T. A. Martinek.** 2007. Performance of the general amber force field in modeling aqueous POPC membrane bilayers. J. Comput. Chem. **28:**2051-2058.

27. **Jorgensen, W. L., J. Chandrasekhar, J. Madura, and M. L. Klein.** 1983. Comparison of simple potential functions for simulating liquid water. J. Chem. Phys. **79:**926-935.

28. **Kandasamy, S. K., and R. G. Larson.** 2006. Molecular dynamics simulations of model trans-membrane peptides in lipid bilayers: a systematic investigation of hydrophobic mismatch. Biophys. J. **90:**2326-2343.

29. **Karplus, M., and J. A. McCammon.** 2002. Molecular dynamics simulations of biomolecules. Nat. Struct. Biol. **9:**646-652.

30. **Kawano, Y., T. Yoshida, K. Hieda, J. Aoki, H. Miyoshi, and Y. Koyanagi.** 2004. A lentiviral cDNA library employing lambda recombination used to clone an inhibitor of human immunodeficiency virus type 1-induced cell death. J. Virol. **78:**11352-11359.

31. **Kerppola, T. K.** 2006. Complementary methods for studies of protein interactions in living cells. Nat. Methods **3:**969-971.

32. **Kerppola, T. K.** 2006. Design and implementation of bimolecular fluorescence complementation (BiFC) assays for the visualization of protein interactions in living cells. Nat. Protoc. **1:**1278-1286.

33. **Kerppola, T. K.** 2006. Visualization of molecular interactions by fluorescence complementation. Nat Rev Mol Cell Biol **7:**449-456.

34. **Klimkait, T., K. Strebel, M. D. Hoggan, M. A. Martin, and J. M. Orenstein.** 1990. The human immunodeficiency virus type 1-specific protein vpu is required for efficient virus

maturation and release. J. Virol. **64:**621-629.

35. **Kollman, P. A., I. Massova, C. Reyes, B. Kuhn, S. Huo, L. Chong, M. Lee, T. Lee, Y. Duan, W. Wang, O. Donini, P. Cieplak, J. Srinivasan, D. A. Case, and T. E. I. Cheatham.** 2000. Calculating structures and free energies of complex molecules: combining molecular mechanics and continuum models. Acc. Chem. Res. **33:**889-897.

36. **Kupzig, S., V. Korolchuk, R. Rollason, A. Sugden, A. Wilde, and G. Banting.** 2003. Bst-2/HM1.24 is a raft-associated apical membrane protein with an unusual topology. Traffic **4:**694-709.

37. **Lefevre, F., M. H. Remy, and J. M. Masson.** 1997. Alanine-stretch scanning mutagenesis: a simple and efficient method to probe protein structure and function. Nucleic Acids Res. **25:**447-448.

38. **Lim, E. S., H. S. Malik, and M. Emerman.** 2010. Ancient adaptive evolution of tetherin shaped the functions of Vpu and Nef in human immunodeficiency virus and primate lentiviruses. J. Virol. **84:**7124-7134.

39. **Loncharich, R. J., B. R. Brooks, and R. W. Pastor.** 1992. Langevin dynamics of peptides: The frictional dependence of isomerization rates of N-actylananyl-N'-methylamide. Biopolymers **32:**523-535.

40. **Maldarelli, F., M. Y. Chen, R. L. Willey, and K. Strebel.** 1993. Human immunodeficiency virus type 1 Vpu protein is an oligomeric type I integral membrane protein. J. Virol. **67:**5056-5061.

41. **Mangeat, B., G. Gers-Huber, M. Lehmann, M. Zufferey, J. Luban, and V. Piguet.** 2009. HIV-1 Vpu neutralizes the antiviral factor Tetherin/BST-2 by binding it and directing its beta-TrCP2-dependent degradation. PLoS Pathog. **5:**e1000574.

42. **Masuyama, N., T. Kuronita, R. Tanaka, T. Muto, Y. Hirota, A. Takigawa, H. Fujita, Y. Aso, J. Amano, and Y. Tanaka.** 2009. HM1.24 is internalized from lipid rafts by clathrin-mediated endocytosis through interaction with alpha-adaptin. J. Biol. Chem. **284:**15927-15941.

43. **McNatt, M. W., T. Zang, T. Hatziioannou, M. Bartlett, I. B. Fofana, W. E. Johnson, S. J. Neil, and P. D. Bieniasz.** 2009. Species-specific activity of HIV-1 Vpu and positive selection of tetherin transmembrane domain variants. PLoS Pathog. **5:**e1000300.

44. **Miaskiewicz, K., R. Osman, and H. Weinstein.** 1993. Molecular dynamics simulation of the hydrated d(CGCGAATTCGCG)2 dodecamer. J. Am. Chem. Soc. **115:**1526–1537.

45. **Montal, M.** 2009. Vpu matchmakers as a therapeutic strategy for HIV infection. PLoS

Pathog. **5:**e1000246.

46. **Neil, S. J., T. Zang, and P. D. Bieniasz.** 2008. Tetherin inhibits retrovirus release and is antagonized by HIV-1 Vpu. Nature **451:**425-430.

47. **Nguyen, K. L., M. llano, H. Akari, E. Miyagi, E. M. Poeschla, K. Strebel, and S. Bour.** 2004. Codon optimization of the HIV-1 vpu and vif genes stabilizes their mRNA and allows for highly efficient Rev-independent expression. Virology **319:**163-175.

48. **Nilsson, L.** 1997. In Encyclopedia of Computational Chemistry. Wiley, New York.

49. **Nyholm, T. K., S. Ozdirekcan, and J. A. Killian.** 2007. How protein transmembrane segments sense the lipid environment. Biochemistry **46:**1457-1465.

50. **Pastor, R. W., B. R. Brooks, and A. Szabo.** 1988. An analysis of the accuracy of Langevin and molecular dynamics algorithms. Mol. Phys. **65:**1409-1419.

51. **Pearlman, D. A., D. A. Case, J. W. Caldwell, W. S. Ross, T. E. I. Cheatham, S. DeBolt, D. Ferguson, G. Seibel, and P. Kollman.** 1995. AMBER, a package of computer programs for applying molecular mechanics, normal mode analysis, molecular dynamics and free energy calculations to simulate the structural and energetic properties of molecules. Comp. Phys. Commun. **91:**1-41.

52. **Poole, E., P. Strappe, H. P. Mok, R. Hicks, and A. M. Lever.** 2005. HIV-1 Gag-RNA interaction occurs at a perinuclear/centrosomal site; analysis by confocal microscopy and FRET. Traffic **6:**741-755.

53. **Ramachandran, G. N., C. Ramakrishnan, and V. Sasisekharan.** 1963. Stereochemistry of polypeptide chain configurations. J. Mol. Biol. **7:**95-99.

54. **Rong, L., J. Zhang, J. Lu, Q. Pan, R. P. Lorgeoux, C. Aloysius, F. Guo, S. L. Liu, M. A. Wainberg, and C. Liang.** 2009. The transmembrane domain of BST-2 determines its sensitivity to down-modulation by human immunodeficiency virus type 1 Vpu. J. Virol. **83:**7536-7546.

55. **Ryckaert, J.-P., G. Ciccotti, and H. J. C. Berendsen.** 1977. Numerical integration of the cartesian equations of motion of a system with constraints: Molecular dynamics of n-alkanes. J. Comput. Phys. **23:**327-341.

56. **Sato, K., S. P. Yamamoto, N. Misawa, T. Yoshida, T. Miyazawa, and Y. Koyanagi.** 2009. Comparative study on the effect of human BST-2/Tetherin on HIV-1 release in cells of various species. Retrovirology **6:**53.

57. **Sauter, D., M. Schindler, A. Specht, W. N. Landford, J. Munch, K. A. Kim, J. Votteler, U. Schubert, F. Bibollet-Ruche, B. F. Keele, J. Takehisa, Y. Ogando, C. Ochsenbauer, J. C.**

Kappes, A. Ayouba, M. Peeters, G. H. Learn, G. Shaw, P. M. Sharp, P. Bieniasz, B. H. Hahn, T. Hatziioannou, and F. Kirchhoff. 2009. Tetherin-driven adaptation of Vpu and Nef function and the evolution of pandemic and nonpandemic HIV-1 strains. Cell Host Microbe **6:**409-421.

58. **Schubert, U., S. Bour, A. V. Ferrer-Montiel, M. Montal, F. Maldarell, and K. Strebel.** 1996. The two biological activities of human immunodeficiency virus type 1 Vpu protein involve two separable structural domains. J. Virol. **70:**809-819.

59. **Schubert, U., and K. Strebel.** 1994. Differential activities of the human immunodeficiency virus type 1-encoded Vpu protein are regulated by phosphorylation and occur in different cellular compartments. J. Virol. **68:**2260-2271.

60. **Shao, J., S. W. Tanner, N. Thompson, and T. E. Cheatham.** 2007. Clustering molecular dynamics trajectories: 1. Characterizing the performance of different clustering algorithms. J. Chem. Theory Comput. **3:**2312–2334.

61. **Shen, L., D. Bassolino, and T. Stouch.** 1997. Transmembrane helix structure, dynamics, and interactions: multi-nanosecond molecular dynamics simulations. Biophys. J. **73:**3-20.

62. **Smith, S. O., M. Eilers, D. Song, E. Crocker, W. Ying, M. Groesbeek, G. Metz, M. Ziliox, and S. Aimoto.** 2002. Implications of threonine hydrogen bonding in the glycophorin A transmembrane helix dimer. Biophys. J. **82:**2476-2486.

63. **Strebel, K., T. Klimkait, and M. A. Martin.** 1988. A novel gene of HIV-1, vpu, and its 16-kilodalton product. Science **241:**1221-1223.

64. **Strebel, K., J. Luban, and K. T. Jeang.** 2009. Human cellular restriction factors that target HIV-1 replication. BMC Med. **7:**48.

65. **Tokarev, A., M. Skasko, K. Fitzpatrick, and J. Guatelli.** 2009. Antiviral activity of the interferon-induced cellular protein BST-2/tetherin. AIDS Res. Hum. Retroviruses **25:**1197-1210.

66. **Ueyama, T., T. Kusakabe, S. Karasawa, T. Kawasaki, A. Shimizu, J. Son, T. L. Leto, A. Miyawaki, and N. Saito.** 2008. Sequential binding of cytosolic Phox complex to phagosomes through regulated adaptor proteins: evaluation using the novel monomeric Kusabira-Green System and live imaging of phagocytosis. J. Immunol. **181:**629-640.

67. **Van Damme, N., D. Goff, C. Katsura, R. L. Jorgenson, R. Mitchell, M. C. Johnson, E. B. Stephens, and J. Guatelli.** 2008. The interferon-induced protein BST-2 restricts HIV-1 release and is downregulated from the cell surface by the viral Vpu protein. Cell Host

Microbe **3:**245-252.

68. **van Meer, G., D. R. Voelker, and G. W. Feigenson.** 2008. Membrane lipids: where they are and how they behave. Nat. Rev. Mol. Cell Biol. **9:**112-124.

69. **Wang, J., R. M. Wolf, J. W. Caldwell, P. A. Kollman, and D. A. Case.** 2004. Development and testing of a general amber force field. J. Comput. Chem. **25:**1157-1174.

70. **Willey, R. L., F. Maldarelli, M. A. Martin, and K. Strebel.** 1992. Human immunodeficiency virus type 1 Vpu protein regulates the formation of intracellular gp160-CD4 complexes. J. Virol. **66:**226-234.

71. **Yoshida, T., H. Ebina, and Y. Koyanagi.** 2009. N-linked glycan-dependent interaction of CD63 with CXCR4 at the Golgi apparatus induces downregulation of CXCR4. Microbiol. Immunol. **53:**629-635.

Table

Table 1. Surface expression of tetherin and its derivatives used in this study.

Name of fusion protein	MFI of tetherin
N-terminally KGC-tagged	
untagged hu-tetherin	107.6±12.7
hu-tetherin	117.6±16.2
KGCstop	13.1±6.8
mo-tetherin	ND
mo(huTM)	ND
mo(huECL)	ND
mo(huCC)	123.3±6.3
mo(huGPI)	ND
hu(muTM)	115.3±4.7
hu(muECL)	138.4±15.0
hu(muCC)	ND
hu(muGPI)	127.9±9.8
LLL(22-24)AAA	116.3±14.6
GIG(25-27)AAA	138.6±27.2
ILV(28-30)AAA	159.4±17.7
LLI(31-33AAA	160.2±19.0
IVI(34-36)AAA	142.1±17.9
LGV (37-39)AAA	161.0±14.1
PLI(40-42)AAA	113.9±12.3
IFT(43-45)AAA	149.8±8.5
IKA(46-48)AAA	117.9±2.0
I34A	155.9 ±5.9
V35A	135.1±34.5
I36A	157.1±18.8
L37A	141.6±26.8
G38A	169.1±23.6
V39A	164.5±14.5
P40A	165.9±4.1
L41A	140.1±9.8
I42A	143.6±29.1

Values indicate the mean of three independent experiments plus standard. ND, not detected

FIGURE LEGENDS

FIG. 1. Interaction of tetherin and Vpu via TM domain.

(A) Schematic diagram of KGN or KGC fusion protein used in this study. KGN- or KGC-peptide-tag was fused in frame to the N-terminus of hu-tetherin, mo-tetherin, or mutant proteins. KGN-tag is fused in frame to the C-terminus of Vpu or its mutant proteins. The L indicates a linker sequence inserted between KG fragments and proteins of interest. Human (white); mouse (black); broken line indicates deletion residues. **(B)** Tetherin-Vpu complex detected by BiFC. HEK293 cells were transfected with the indicated DNA and examined by confocal microscopy (upper panels) and immunoblot analysis (lower panels). **(C)** BiFC-expressing cells were stained with markers specific for each organelle and imaged by confocal microscopy. Bar, 10μm. The ratio of the merged area between BiFC (green) and organelles (red) were quantified (right columns) for more than one hundred cells. **(D)** Quantitative BiFC assay. The KGN-Vpu-expressing cells were transfected with pKGC-hu-tetherin (0, 100, 200 or 400 ng) or a control (pKGC-hu-tetherin(-) 400 ng) and analyzed by flow cytometry (upper columns) and immunoblot analysis (lower panels) . Relative MFI are defined as (MFI of tetherin plasmid-transfected cells) – (MFI of untransfected cells), and results represent the mean of three independent experiments plus standard (Fig. D).

Figure 2. Interaction of tetherin and Vpu via TM domains.

(A) The KGN-Vpu-expressing cells were transfected with plasmid encoding KGC-tagged hu-tetherin or deletion-mutants of CT or GPI (delCT and delGPI). The expression of KGC-tetherin fusion protein was detected using an anti-KGC antibody (bottom panels). Relative MFI is defined as (MFI of pKGC-tetherin- or its mutants-transfected cells) – (MFI of untransfected cells), and results represent the mean of three independent experiments plus standard. The amount of protein applied for the delGPI WB was ten times-less than WT hu-tetherin to avoid overexposure of the protein on polyvinylidene difluoride membrane. Statistical significance (Student's t-test) in the MFI of human tetherin and mutants are represented as follows: $^{**}P < 0.01$ $^{*}P < 0.05$.

(B**)** The KGN-Vpu-expressing HEK293 cells were transfected with pKGC-mo-tetherin (upper panels) or pKGC-hu-tetherin (lower panels). Cells were double stained with anti-Vpu antibody and anti-KGC antibody, and imaged by confocal microscopy.

(C) Interaction of tetherin TM with Vpu. The KGN-Vpu-expressing cells were transfected with the KGC-hu-tetherin, KGC-mo-tetherin or the chimera mutant DNA containing

reciprocal exchanges of the TM, ECL, CC, or GPI between the hu- and mo- tetherin proteins and analyzed by flow cytometry. Statistical significance (Student's t-test) in the MFI of hu-tetherin and chimeras are represented as follows: * $P < 0.01$, SD of mo(huCC)=0.0061. Relative MFI is defined as (MFI of pKGC-tetherin- or its mutants-transfected cells) – (MFI of untransfected cells)

(D) Interaction of the Vpu TM with tetherin. KGC-tetherin-expressing cells were transfected with KGN-Vpu or its mutant DNA and analyzed. Statistical significance (Student's t-test) in the BiFC signals are represented as values. Relative MFI are defined as (MFI of pKGN-Vpu or its mutant transfected cells) – (MFI of untransfected cell MFI). The results represent the mean of three independent experiments (A, C, D). Expression of KGC- or KGN-fusion, or Vpu protein was detected by immunoblot analysis with individual antibodies (A, C, D).

FIG. 3. The AA residues of hu-tetherin TM region required for Vpu interaction and counteraction.

(A and B) BiFC assay of hu-tetherin TM mutants on Vpu interaction. Schematic diagram showing the AA substitutions made in the C-terminal TM region of hu-tetherin. Identity is indicated by dashes. The KGN-Vpu-expressing cells were transfected with a series of KGC-hu-tetherin TM mutants and analyzed by flow cytometry as described in Materials and Methods. Protein expression of KGC fused hu-tetherin and its mutants in cell lysates were detected using indicated antibody. Relative MFI are defined as (MFI of pKGN-Vpu- or its mutants-transfected cells) – (MFI of untransfected cell), and results represent the mean of three independent experiments plus standard. **(C)** Tetherin activity and Vpu sensitivity of hu-tetherin TM mutants. HEK 293 cells were co-transfected with WT HIV-1 infectious DNA (pNL4-3) or its *vpu*-deleted DNA (pNL4-3/Udel) (1 μg) with or without (Control) pKGC-hu-tetherin and its derivative expression plasmids (100 ng). The expression of HIV-1 ($Pr55^{Gag}$) in the cell lysates were detected using anti-p24 antibody. Results represent the mean of more than three independent experiments. Statistical significance (Student's t-test) is represented as *, $P < 0.05$; ** $P < 0.01$ **(A), (B) and (D)** or values **(C)**. **(D) S**urface expression of tetherin and its mutants. HEK 293 cells were co-transfected with WT HIV-1 infectious DNA (pNL4-3) or its *vpu*-deleted DNA (pNL4-3/Udel) (1 μg) with or without (Control) pKGC-hu-tetherin and its mutant expression plasmids (100 ng). The cell surface expression of tetherin was detected using anti-tetherin antibody. **(E)** AA alignment of seven primates and mo-tetherin TM domain.

Identity is indicated by dashes, and sequence gaps are indicated by an asterisk. Gray boxes indicate AA sequences corresponding to the mutants that the BiFC signals were significantly decreased.

FIG. 4. C-terminal motif in tetherin TM domain is a determinant for Vpu counteraction.

(A) AA alignment of hu-tetherin, agm-tetherin and their mutants. Identity is indicated by dashes, and sequence gaps are indicated by an asterisk. **(B)** Subcellular localization of tetherin 2AA deletion-mutant or insertion-mutant. KGN-Vpu-expressing cells were transfected with plasmid encoding KGC-tagged hu-tetherin, KGC-tagged agm-tetherin, or their mutants, respectively, and cells were stained with an anti-KGC antibody. Interferon-treated HEK293 cells were stained with an anti-tetherin antibody. Cells were examined by confocal microscopy. **(C)** BiFC assay of hu- and agm-tetherin TM mutants on Vpu interaction. KGN-Vpu-expressing cells were transfected with plasmid encoding KGC-hu-tetherin, KGC-agm-tetherin, or these mutants and analyzed by flow cytometry. The expression of the protein in cell lysates was detected using indicated antibody. Relative MFI are defined as (MFI of pKGC-tetherin or its mutant transfected cells) – (MFI of untransfected cell), and results represent the mean of three independent experiments plus standard. **(D)** Tetherin activity and Vpu sensitivity assays of hu- and agm-tetherin TM mutants. HEK 293 cells were co-transfected as described in Fig. 2B with 100 ng or without (Control) KGC-hu-tetherin or agm-tetherin and these derivatives DNA. The HIV-1 proteins ($Pr55^{Gag}$) in the cell lysates were detected using an anti-p24 antibody. Results represent the mean of three independent experiments plus standard. Values represent the statistical significance (Student's t test).

FIG. 5. Structure model of tetherin TM domains

(A) Structural models of C-terminal TM domains (G27 to E51 in hu-tetherin). I34, L37, and L41 whose mutations influence interactions with Vpu are highlighted with red cartoon and sticks. V30, F44, T45, and A48 whose side chains are positioned in the same face with side chains of I34, L37, and L41 are highlighted with orange cartoon and sticks. **(B)** Comparisons of three-dimensional structures of individual residues between hu-tetherin and others. RMSD values between hu-tetherin and other models were calculated using the coordinates of N, Cα, and C atoms in the C-terminal TM domain (G27 to E51 in hu-tetherin) in the representative structures, each of which were selected from 3,000 snapshots during 2.0-5.0 nanoseconds of the respective MD simulations using the Bayesian

clustering algorithm. The individual residues in the structures were colored according to the RMSD values. The three-dimensional images of the structures were made with PyMOL ver. 0.99 rc6 (Schrödinger LLC, http://www.pymol.org/).

FIG.1

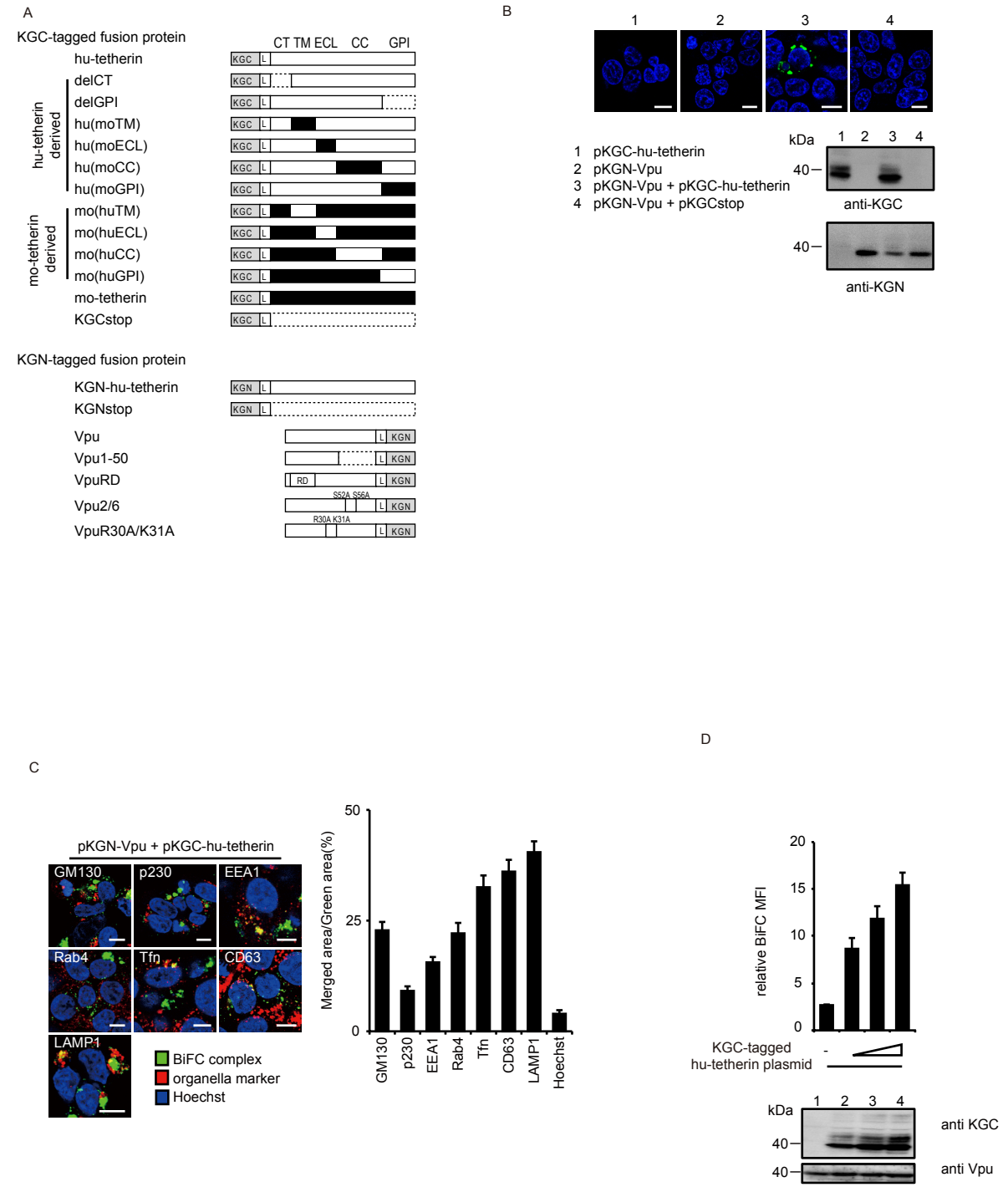
A
KGC-tagged fusion protein
CT TM ECL CC GPI
hu-tetherin
delCT
delGPI
hu(moTM)
hu(moECL)
hu(moCC)
hu(moGPI)
hu-tetherin derived
mo(huTM)
mo(huECL)
mo(huCC)
mo(huGPI)
mo-tetherin derived
mo-tetherin
KGCstop
KGC
L
KGN-tagged fusion protein
KGN-hu-tetherin
KGNstop
KGN
Vpu
Vpu1-50
VpuRD
RD
Vpu2/6
S52A S56A
VpuR30A/K31A
R30A K31A
B
1
2
3
4
kDa
1 pKGC-hu-tetherin
2 pKGN-Vpu
3 pKGN-Vpu + pKGC-hu-tetherin
4 pKGN-Vpu + pKGCstop
40
anti-KGC
anti-KGN
C
pKGN-Vpu + pKGC-hu-tetherin
GM130
p230
EEA1
Rab4
Tfn
CD63
LAMP1
BiFC complex
organella marker
Hoechst
Merged area/Green area(%)
50
25
0
GM130
p230
EEA1
Rab4
Tfn
CD63
LAMP1
Hoechst
D
relative BiFC MFI
20
15
10
5
0
KGC-tagged hu-tetherin plasmid
-
kDa
1 2 3 4
40
40
anti KGC
anti Vpu

FIG. 2

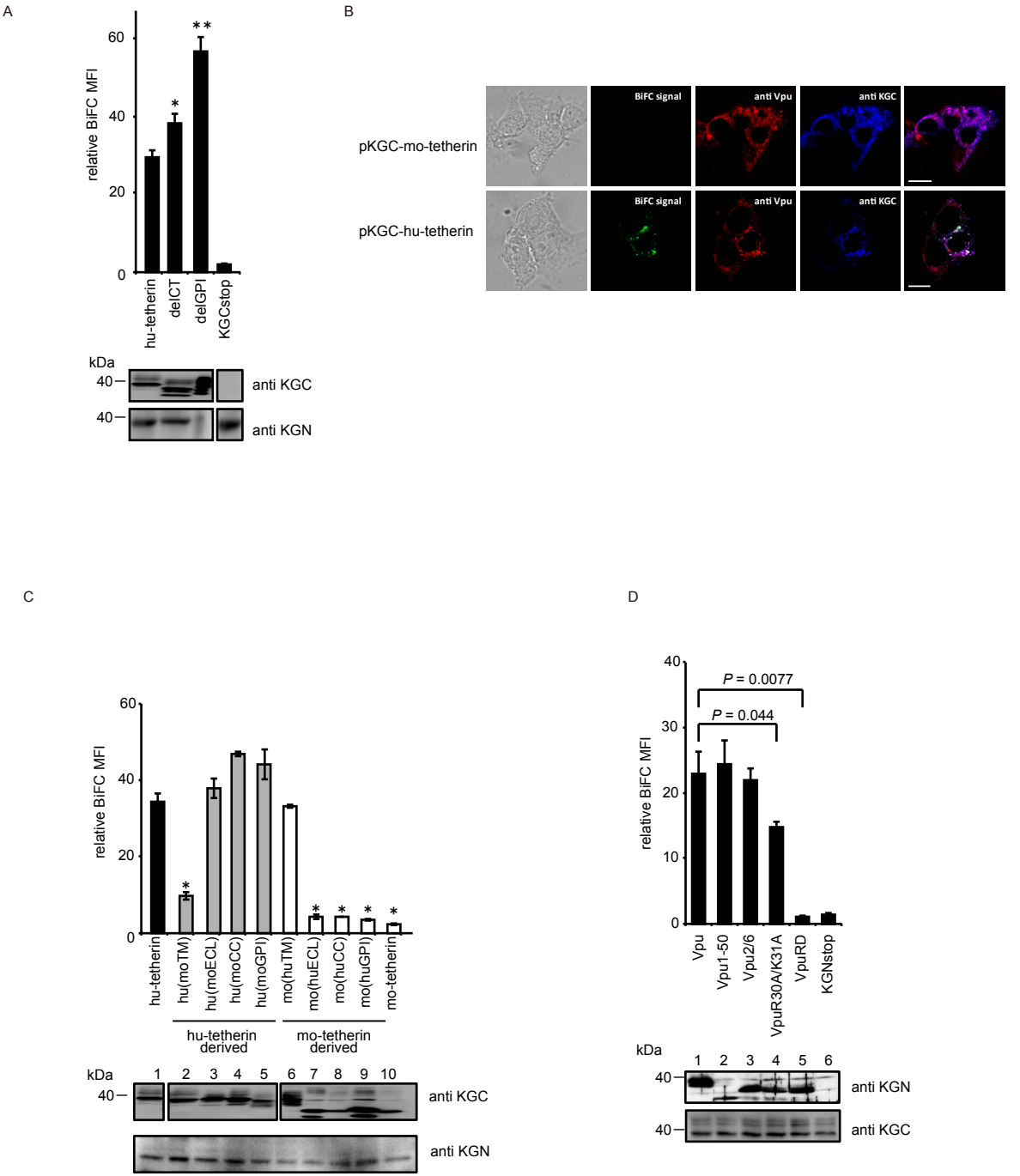
A
relative BiFC MFI
60
40
20
0
**
*
hu-tetherin
delCT
delGPI
KGCstop
kDa
40
anti KGC
40
anti KGN
B
pKGC-mo-tetherin
pKGC-hu-tetherin
BiFC signal
anti Vpu
anti KGC
C
relative BiFC MFI
60
40
20
0
hu-tetherin
hu(moTM)
hu(moECL)
hu(moCC)
hu(moGPI)
mo(huTM)
mo(huECL)
mo(huCC)
mo(huGPI)
mo-tetherin
hu-tetherin derived
mo-tetherin derived
kDa
1 2 3 4 5 6 7 8 9 10
40
anti KGC
anti KGN
D
relative BiFC MFI
40
30
20
10
0
P = 0.0077
P = 0.044
Vpu
Vpu1-50
Vpu2/6
VpuR30A/K31A
VpuRD
KGNstop
kDa
1 2 3 4 5 6
40
anti KGN
40
anti KGC

FIG. 3

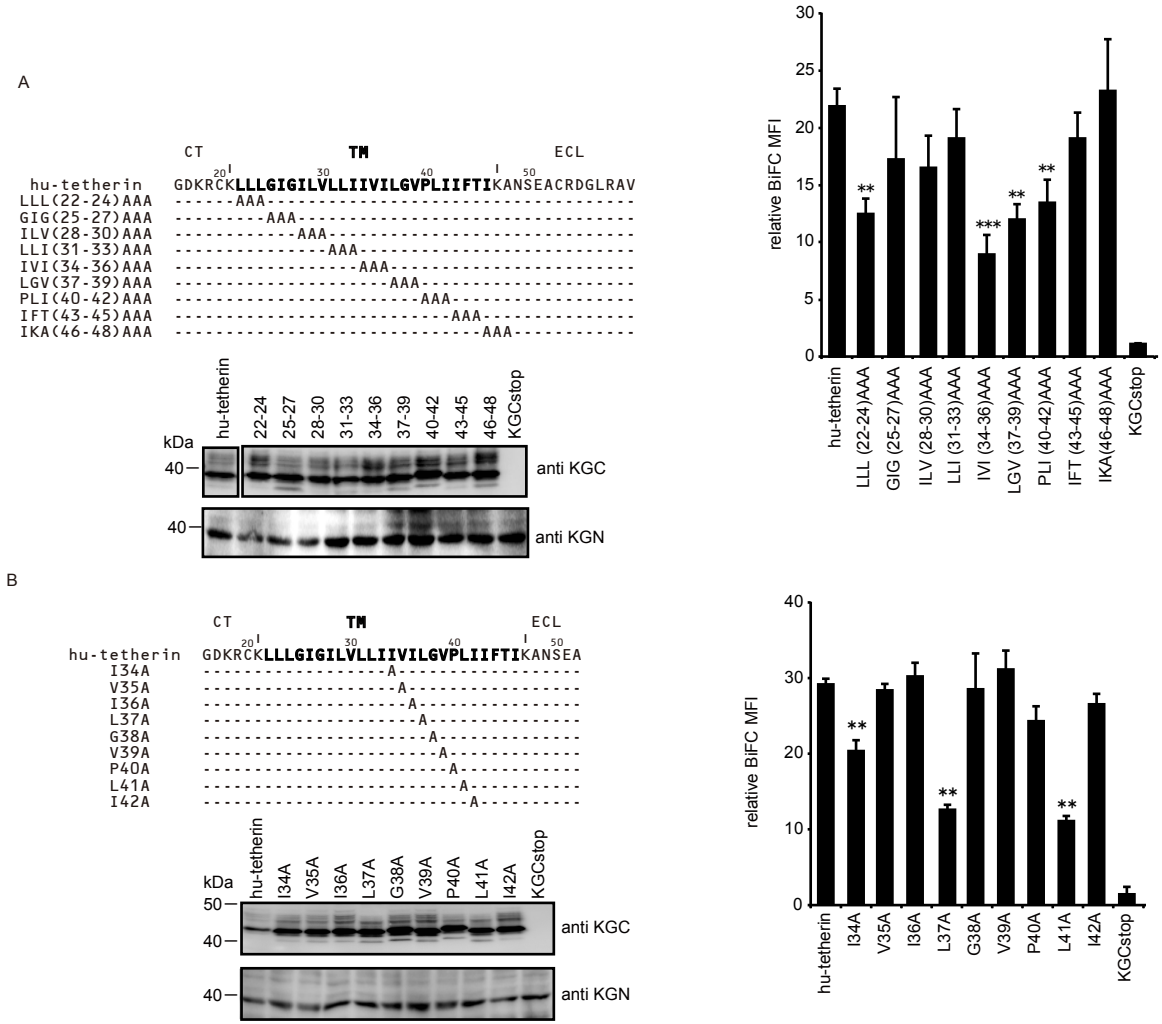
A
CT
TM
ECL
hu-tetherin GDKRCKLLLGIGILVLLIIVILGVPLIIFTIKANSEACRDGLRAV
LLL(22-24)AAA
GIG(25-27)AAA
ILV(28-30)AAA
LLI(31-33)AAA
IVI(34-36)AAA
LGV(37-39)AAA
PLI(40-42)AAA
IFT(43-45)AAA
IKA(46-48)AAA
hu-tetherin
22-24
25-27
28-30
31-33
34-36
37-39
40-42
43-45
46-48
KGCstop
kDa
40
anti KGC
anti KGN
relative BiFC MFI
B
hu-tetherin GDKRCKLLLGIGILVLLIIVILGVPLIIFTIKANSEA
I34A
V35A
I36A
L37A
G38A
V39A
P40A
L41A
I42A
KGCstop
50
40

FIG. 3

C

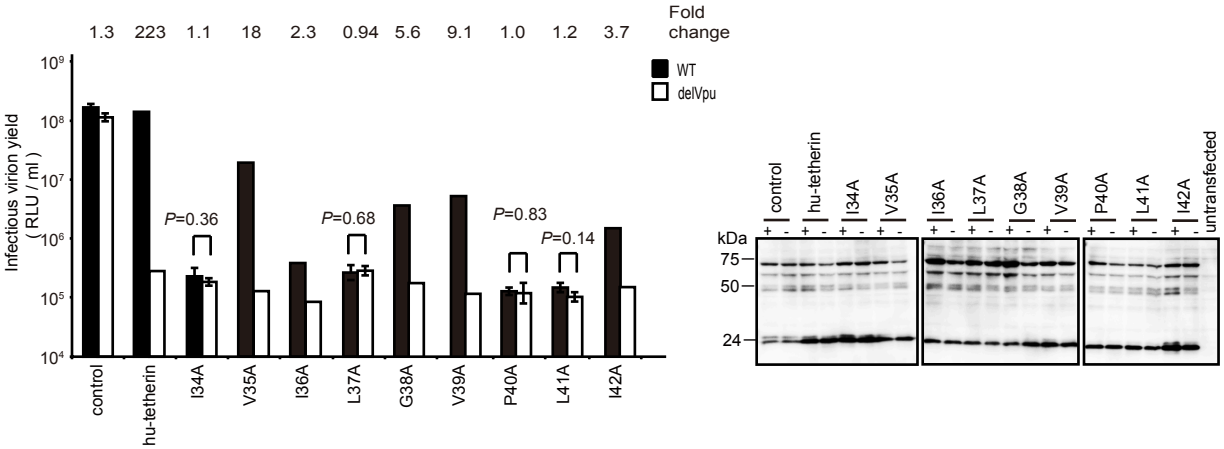
Fold change
1.3 223 1.1 18 2.3 0.94 5.6 9.1 1.0 1.2 3.7
WT
delVpu
Infectious virion yield (RLU / ml)
P=0.36
P=0.68
P=0.83
P=0.14
control
hu-tetherin
I34A
V35A
I36A
L37A
G38A
V39A
P40A
L41A
I42A
kDa
75
50
24
untransfected

D

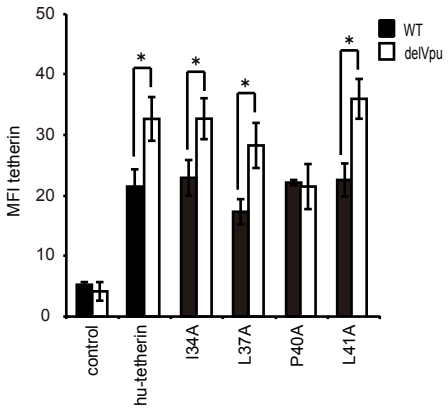
WT
delVpu
MFI tetherin
control
hu-tetherin
I34A
L37A
P40A
L41A

E

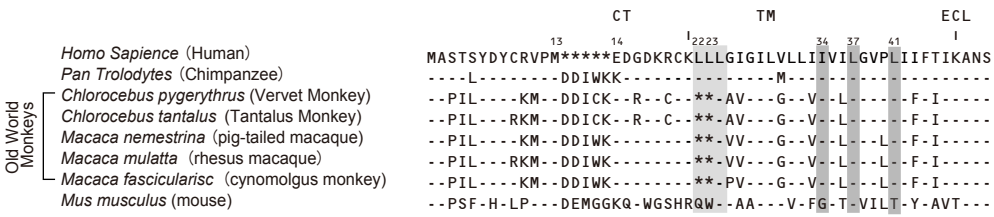
CT
TM
ECL
Homo Sapience (Human)
Pan Trolodytes (Chimpanzee)
Old World Monkeys
Chlorocebus pygerythrus (Vervet Monkey)
Chlorocebus tantalus (Tantalus Monkey)
Macaca nemestrina (pig-tailed macaque)
Macaca mulatta (rhesus macaque)
Macaca fascicularisc (cynomolgus monkey)
Mus musculus (mouse)
MASTSYDYCRVPM*****EDGDKRCKLLLGIGILVLLIIVILGVPLIIFTIKANS

FIG. 4

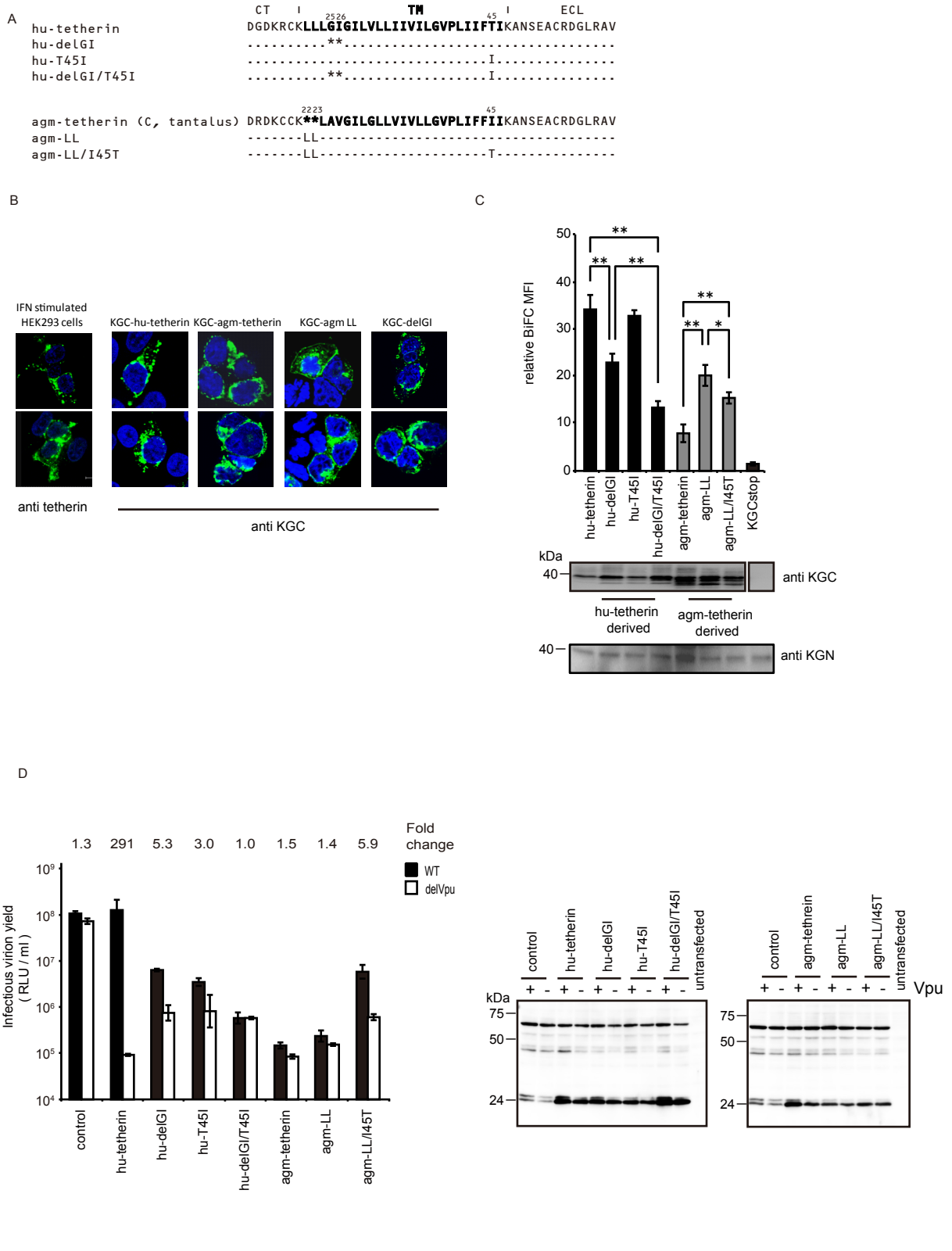
A
CT
TM
ECL
hu-tetherin DGDKRCKLLLGIGILVLLIIVILGVPLIIFTIKANSEACRDGLRAV
hu-delGI ....**.....
hu-T45I .....I.....
hu-delGI/T45I ..........**.....I.....
agm-tetherin (C, tantalus) DRDKCCK**LAVGILGLLVIVLLGVPLIFFIIKANSEACRDGLRAV
agm-LL -------LL-----
agm-LL/I45T -------LL-----T-----
B
IFN stimulated HEK293 cells
KGC-hu-tetherin
KGC-agm-tetherin
KGC-agm LL
KGC-delGI
anti tetherin
anti KGC
C
relative BiFC MFI
hu-tetherin
hu-delGI
hu-T45I
hu-delGI/T45I
agm-tetherin
agm-LL
agm-LL/I45T
KGCstop
kDa
anti KGC
hu-tetherin derived
agm-tetherin derived
anti KGN
D
Fold change
1.3 291 5.3 3.0 1.0 1.5 1.4 5.9
WT
delVpu
Infectious virion yield (RLU / ml)
control
hu-tetherin
hu-delGI
hu-T45I
hu-delGI/T45I
agm-tetherin
agm-LL
agm-LL/I45T
untransfected
agm-tethrein
Vpu
kDa

FIG. 5

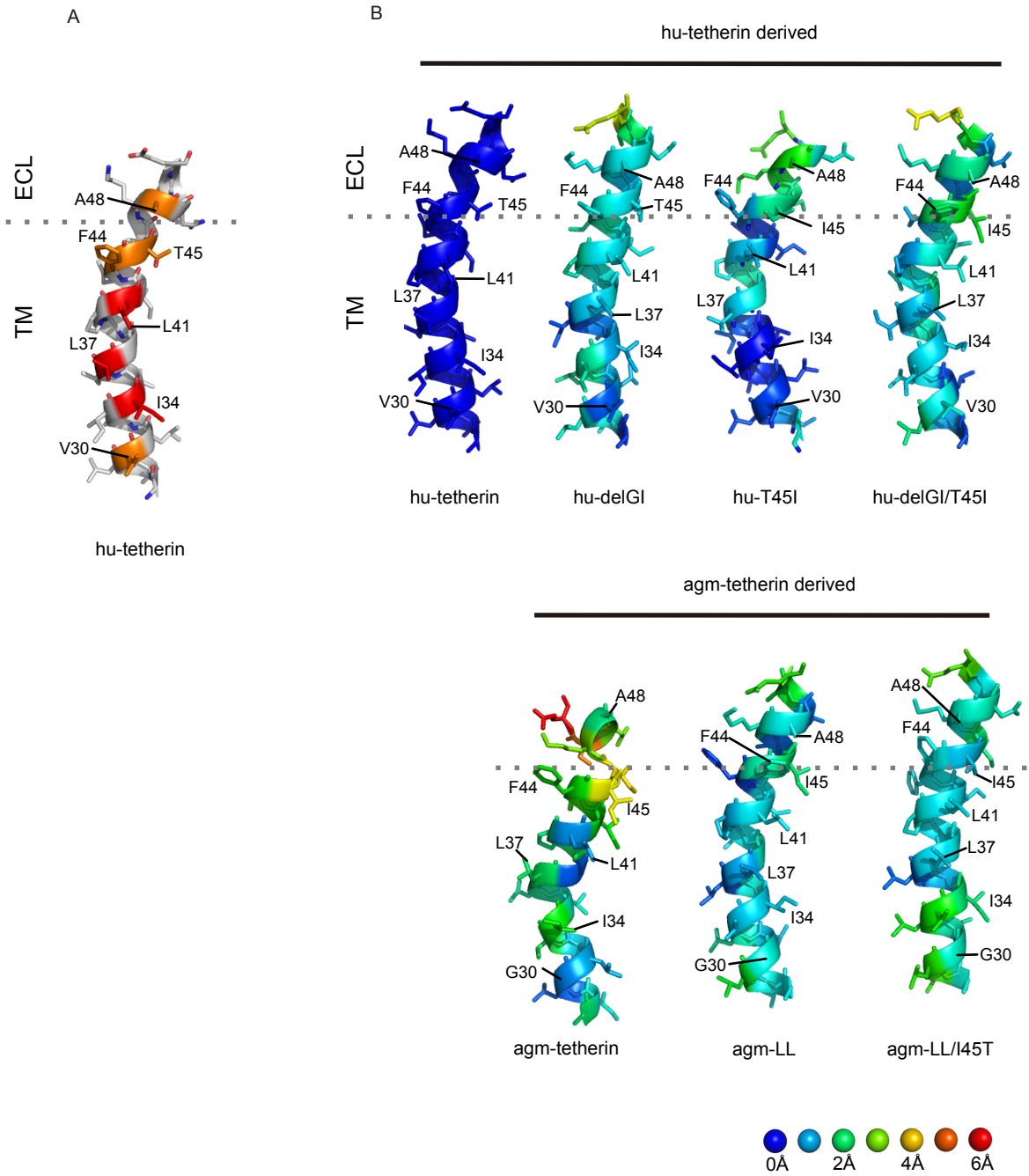
A
ECL
TM
A48
F44
T45
L41
L37
I34
V30
hu-tetherin
B
hu-tetherin derived
ECL
TM
A48
F44
T45
L41
L37
I34
V30
hu-tetherin
hu-delGI
hu-T45I
hu-delGI/T45I
I45
agm-tetherin derived
G30
agm-tetherin
agm-LL
agm-LL/I45T
0Å
2Å
4Å
6Å

SUPPLEMENTAL MATERIAL

Supplementary Table

Table S1. RMSD values of most frequently observed conformations to other four conformations during 2.0-5.0 nano seconds of molecular dynamics simulations in each model.

	hu-tetherin		agm-tetherin		agm-LL		agm-LL/I45T		hu-delGI		hu-T45I		hu-delGI/T45I	
Cluster	Freq (%)	RMSD (Å)	Freq (%)	RMSD (Å)	Freq (%)	RMSD (Å)	Freq (%)	RMSD (Å)	Freq (%)	RMSD (Å)	Freq (%)	RMSD (Å)	Freq (%)	RMSD (Å)
1	34.1		25.7		23.2		27.3		31.1		22.0		32.2	
2	21.1	1.11 (1.37)*	24.5	0.50 (1.38)	21.8	1.39 (2.03)	24.2	0.48 (1.80)	27.6	0.64 (0.77)	21.7	1.12 (1.60)	29.6	0.61 (0.98)
3	20.7	1.55 (2.94)	23.3	0.70 (0.99)	21.5	0.79 (0.93)	18.3	0.45 (1.15)	16.3	0.62 (0.80)	20.2	1.20 (1.91)	18.2	0.65 (1.17)
4	14.7	0.82 (1.56)	14.9	1.39 (1.68)	17.1	1.51 (2.05)	16.5	0.51 (1.26)	15.3	0.59 (0.66)	20.0	1.18 (2.73)	10.1	0.71 (0.93)
5	9.5	1.67 (2.68)	11.5	1.99 (3.05)	16.4	1.01 (1.17)	13.8	0.57 (0.76)	9.7	0.43 (0.85)	16.1	0.89 (1.56)	9.8	0.86 (1.13)

The 3,000 snapshots were clustered into five groups with Bayesian algorithm. The RMSD values were calculated when the conformations were fitted using the coordinates of N, Cα, and C atoms in the region corresponding to that between G27 and E51 in hu-tetherin.

* The values in parentheses show the RMSD when the conformations were fitted using the coordinates of N, Cα, and C atoms in all residues (D15-C53 in hu-tetherin).

FIGURE LEGENDS

Supplemental Figure 1. Time course of changes in structures during molecular dynamics simulations. Green line shows the RMSD values of peptides in each model and red line shows the membrane thickness.

Supplemental Figure 2. Comparisons of three-dimensional structures of individual residues at C-terminal TM regions (G27 to E51 in hu-tetherin) between hu-tetherin and others.

(A) Analyses for agm-tetherin variants. **(B)** Analyses for hu-tetherin variants. RMSD values between hu-tetherin and other models were calculated using each representative structure in 3,000 snapshots during 2.0-5.0 nanoseconds of the respective MD simulations as described in Fig. 4A. Bottom sequences in the graphs indicated the sequence of hu-tetherin. Parts with red and orange background in each graph highlight residues colored red and orange in Fig. 4A, respectively.

Supplemental Figure 3. Structure at C-terminal TM domain (G27 to E51 in hu-tetherin) in the final snapshot of each MD simulation at 5 nanosecond.

(A) Structure of C-terminal TM domains (G27 to E51 in hu-tetherin) for hu-tetherin. I34, L 37, and L41 whose mutations influence interactions with Vpu were highlighted with red cartoon and sticks. V30, F44, T45, and A48 whose side chains were positioned in the same face with side chains of I34, L37, and L41 were highlighted with orange cartoon and sticks. **(B)** Comparisons of three-dimensional structures of individual residues between hu-tetherin and others. RMSD values between hu-tetherin and others were calculated using the coordinates of N, Cα, and C atoms in the C-terminal TM domain (G27 to E51 in hu-tetherin) in the representative structures, each of which was the final snapshot the respective MD simulations. The individual residues in the structures were colored according to the RMSD values. The three-dimensional images of the structures were made with PyMOL ver. 0.99 rc6 (Schrödinger LLC, http://www.pymol.org/).

FIG. S1

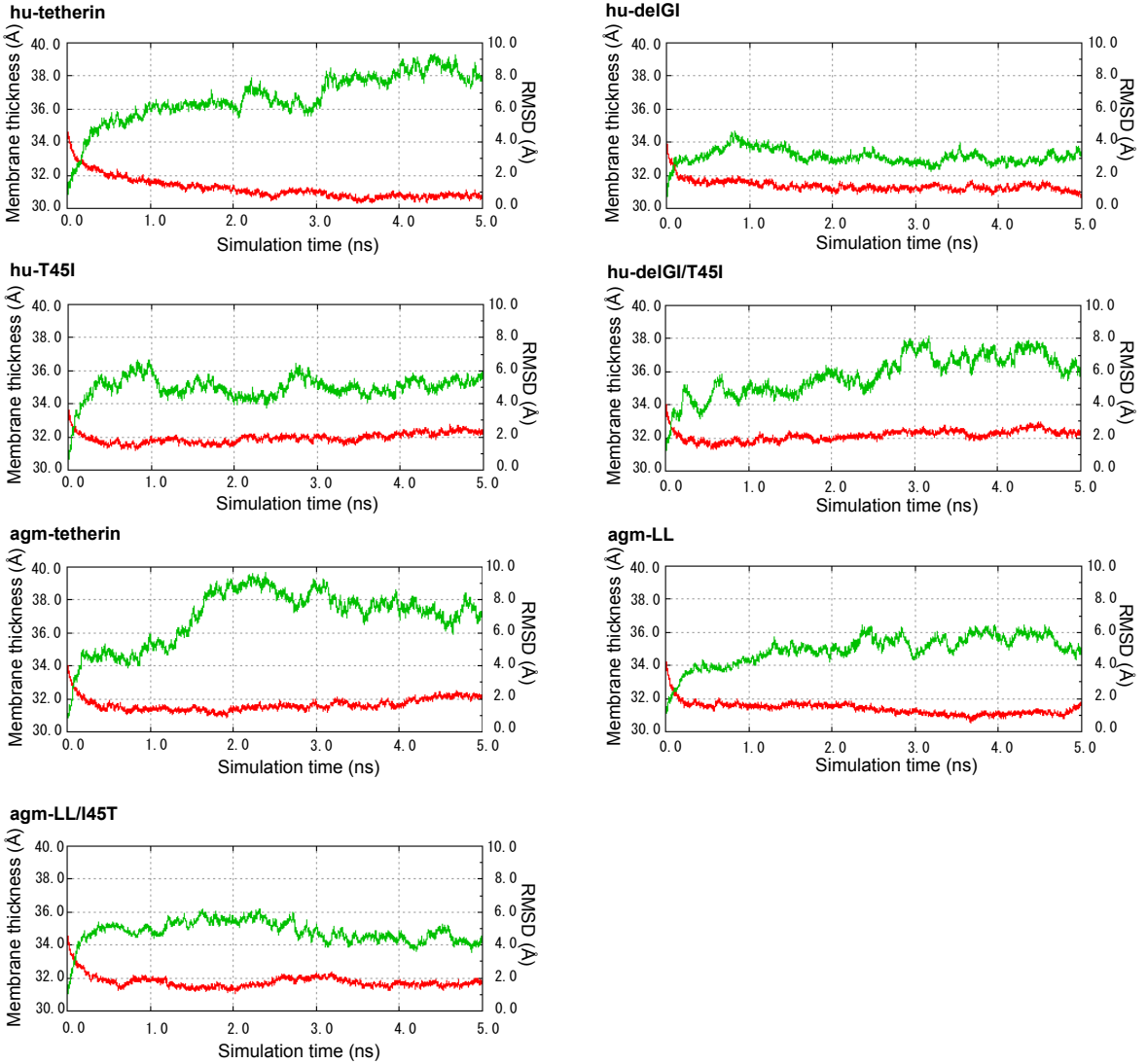
hu-tetherin
hu-delGl
hu-T45I
hu-delGl/T45I
agm-tetherin
agm-LL
agm-LL/I45T
Membrane thickness (Å)
RMSD (Å)
Simulation time (ns)

FIG. S2

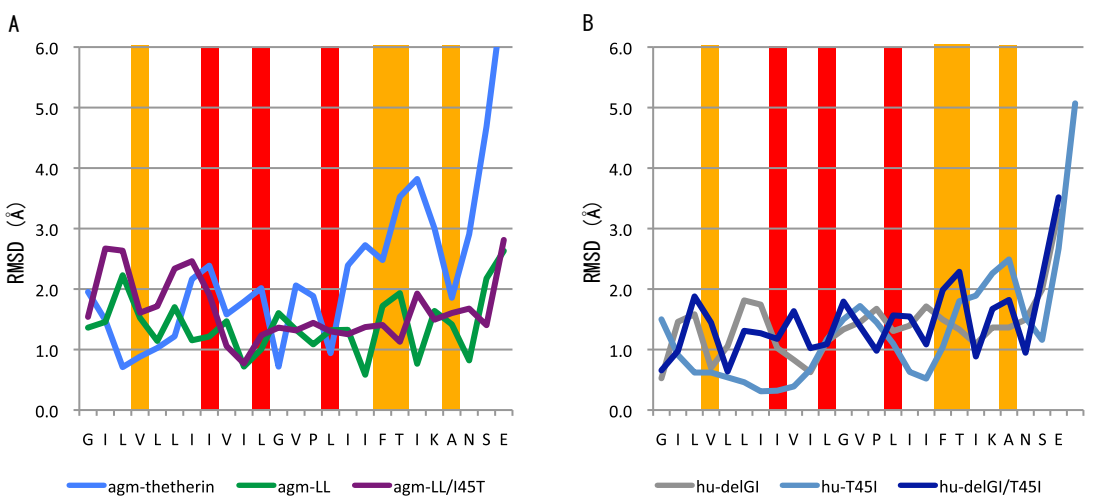
A
B
RMSD (Å)
G I L V L L I I V I L G V P L I I F T I K A N S E
agm-tetherin
agm-LL
agm-LL/I45T
hu-delGl
hu-T45I
hu-delGl/T45I

FIG. S3

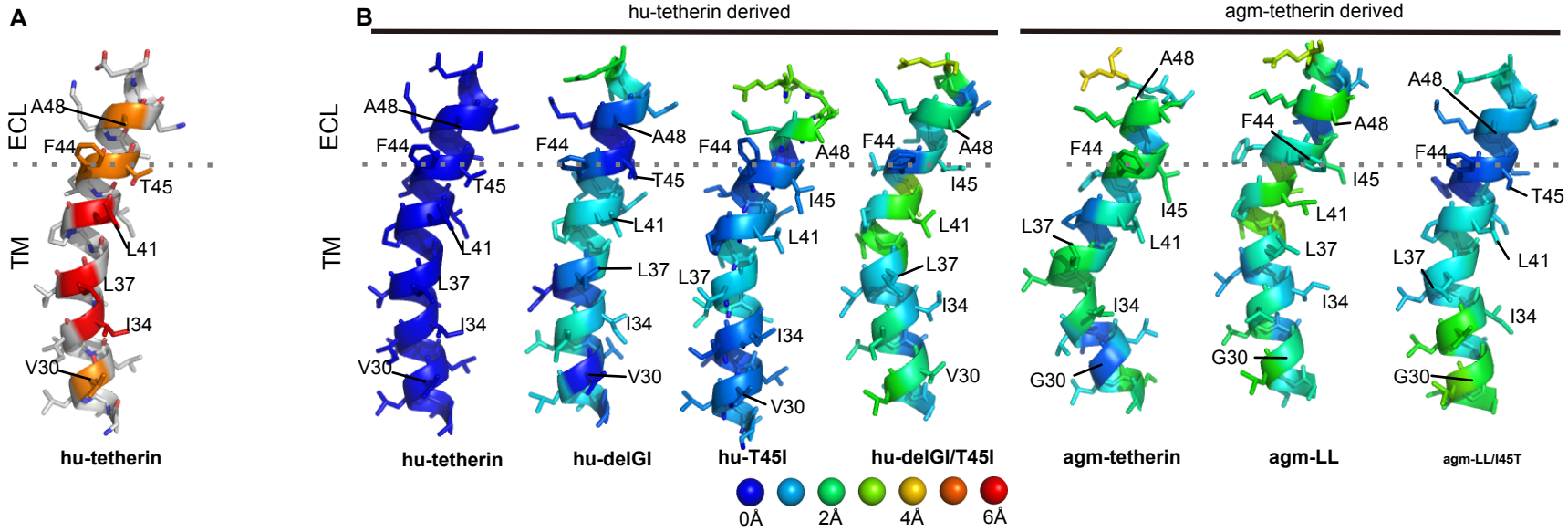
A
ECL
TM
A48
F44
T45
L41
L37
I34
V30
hu-tetherin
B
hu-tetherin derived
agm-tetherin derived
hu-tetherin
hu-delGI
hu-T45I
hu-delGI/T45I
agm-tetherin
agm-LL
agm-LL/I45T
0Å
2Å
4Å
6Å